

9-30-1990

## A detailed mechanism for initial phases of oxidation and pyrolysis of methyl tert-butyl ether (MTBE)

Wen-Chiun Ing  
*New Jersey Institute of Technology*

Follow this and additional works at: <https://digitalcommons.njit.edu/theses>

 Part of the [Environmental Sciences Commons](#)

---

### Recommended Citation

Ing, Wen-Chiun, "A detailed mechanism for initial phases of oxidation and pyrolysis of methyl tert-butyl ether (MTBE)" (1990). *Theses*. 2759.

<https://digitalcommons.njit.edu/theses/2759>

This Thesis is brought to you for free and open access by the Electronic Theses and Dissertations at Digital Commons @ NJIT. It has been accepted for inclusion in Theses by an authorized administrator of Digital Commons @ NJIT. For more information, please contact [digitalcommons@njit.edu](mailto:digitalcommons@njit.edu).

## **Copyright Warning & Restrictions**

The copyright law of the United States (Title 17, United States Code) governs the making of photocopies or other reproductions of copyrighted material.

Under certain conditions specified in the law, libraries and archives are authorized to furnish a photocopy or other reproduction. One of these specified conditions is that the photocopy or reproduction is not to be “used for any purpose other than private study, scholarship, or research.” If a user makes a request for, or later uses, a photocopy or reproduction for purposes in excess of “fair use” that user may be liable for copyright infringement,

This institution reserves the right to refuse to accept a copying order if, in its judgment, fulfillment of the order would involve violation of copyright law.

**Please Note: The author retains the copyright while the New Jersey Institute of Technology reserves the right to distribute this thesis or dissertation**

Printing note: If you do not wish to print this page, then select “Pages from: first page # to: last page #” on the print dialog screen

The Van Houten library has removed some of the personal information and all signatures from the approval page and biographical sketches of theses and dissertations in order to protect the identity of NJIT graduates and faculty.

## ABSTRACT

**Title of Thesis:** A Detailed Mechanism for Initial Phases  
of Oxidation and Pyrolysis of  
Methyl *Tert*-Butyl Ether(MTBE)

**Name:** Wen-Chiun Ing  
Master of Science in Environmental Science.

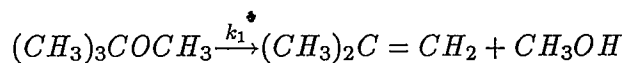
**Thesis directed by:** Dr. J. W. Bozzelli

The lead phasedown in gasoline in both the U. S. and in Europe, the failure of other nonlead oxygenates (e.g. ethanol...) to significantly improve octance ratings and therefore to serve as replacement for tetra ethyl lead in gasoline, and the U. S. Environmental Protection Agency's restrictions on gasoline RVP (Reid Vapor Pressure) to decrease tropospheric ozone concentrations are the factors causing the rapid growth in MTBE demand. There is however no detailed chemical kinetic study on the thermal or oxidative reactions of MTBE for full understanding the behavior and characteristics of MTBE and its degradation products during combustion processes.

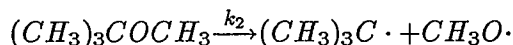
Detailed mechanisms were developed for the oxidation reactions of MTBE (methyl *tert*-butyl ether) and compared with the experimental data done by Norton et.al.<sup><14></sup> in this work. The unimolecular and bimolecular including chemical activation processes versions of Quantum RRK theory were used to develop kinetic mechanisms for the MTBE oxidations. Sensitivity analysis on this reaction

mechanism was performed to identify the important reaction channels and to improve the fit of the mechanism on experimental observation.

The model results give a satisfactory fit for the conversion of MTBE with the experimental data. This mechanism clearly indicates the acceptable path toward the formation of the major experimentally observed products, isobutylene and methanol. The molecular elimination path is dominant when temperature are below  $\sim 900$  K in the MTBE oxidation system. Our mechanism explains why Daly *et al.*<sup><24></sup> and Choo *et al.*<sup><25></sup> concluded that the decomposition reaction of MTBE is a four-center molecular elimination at the condition of temperature around 700 K. We determine rate constants for important reactions at 1 atm and temperature between 800 and 1200 K :



$$k_1 = 7.72 \times 10^{13} \exp(-29700/T) \text{ sec}^{-1}$$



$$k_2 = 3.66 \times 10^{17} \exp(-39600/T) \text{ sec}^{-1}$$

The difference between the calculation result and high pressure limit increases when the temperature is above 1000 K at atmospheric pressure. The reaction of  $(C_3CO \rightarrow C_3C \cdot + CH_3O \cdot)$  therefore becomes important as the temperature increasing and becomes dominant when the temperature is higher than 1800 K.

## APPROVAL OF THESIS

Title of Thesis : A Detailed Mechanism for Initial Phases  
of Oxidation and Pyrolysis of  
Methyl *Tert*-Butyl Ether(MTBE).

Name of Candidate : Wen-Chiun Ing  
Master of Science in Environmental Science

Thesis and Abstract approved by :

---

Dr. J. W. Bozzelli  
Professor of Chemical Engineering  
Department of Chemical Engineering,  
Chemistry & Environmental Science

Sept 17/90  
Date

---

Dr. R. Trattner  
Professor of Environmental Science & Chemistry  
Department of Chemical Engineering,  
Chemistry & Environmental Science

9/18/90  
Date

---

Dr. H. Shaw  
Professor of Chemical Engineering  
Department of Chemical Engineering,  
Chemistry & Environmental Science

Sept 17, 1990  
Date

## VITA

Name : Wen-Chiun Ing

Degree & Date : Master of Science in Environmental Science  
1990

Present address :

Date of Birth :

Place of Birth :

Secondary education : Shang-Uang high school

Collegiate Institute	Date	Degree	Date Graduated
National Taipei Institute of Technolodge	1978-1983	B.S Ch.E	May, 1983
New Jersey Institute of Technology	1987-1989	M.S En.Sc.	Oct., 1990

Major : Environmental Science

Position Held :

1988-1990 : Research Assistant in NJIT, NJ

1986-1988 : Section Leader, Shift Supervisor  
in Shin-kon Sythetic Fibre Corp. Taiwan R.O.C.

# Contents

<b>1</b>	<b>Introduction</b>	<b>1</b>
<b>2</b>	<b>Previous Studies</b>	<b>4</b>
<b>3</b>	<b>Theory</b>	<b>8</b>
3.1	Transition State and Collision Theory . . . . .	8
3.2	Prediction of Rate Constants Reaction by Unimolecular and Bimolecular QRRK Theory . . . . .	13
<b>4</b>	<b>Results and Discussion</b>	<b>22</b>
4.1	Important Reactions . . . . .	22
4.2	Important Dissociation Reactions . . . . .	29
4.3	Kinetic Mechanism and Modeling . . . . .	59
<b>5</b>	<b>Conclusion</b>	<b>76</b>
<b>6</b>	<b>Reference</b>	<b>78</b>

<b>A Species in Reaction Mechanism</b>	<b>81</b>
<b>B DISSOC Input Data and Results</b>	<b>84</b>

# Chapter 1

## Introduction

"We believe that during the 1990s, methyl *tert*-butyl ether (MTBE) will be one of the fastest growing chemicals in the world," said Sabic Marketing Ltd. Pres. Abdullah S. Nojaidi<sup><1></sup>. Between 1980, the first year in which the U. S. International Trade Commission began reporting separate data on MTBE, and 1984, production has grown at an annual compound rate of 20%<sup><2></sup>. U. S. consumption of MTBE has been reported to be growing at a rate of 40% per year in 1986<sup><3></sup>. About forty plants are running and thirty more are under construction or planned<sup><1></sup> including three plants which will be built in Canada with a total capacity of 1.5 million metric tons<sup><4>,<5></sup>. If all planned projects(1987) are built, MTBE production will reach about 20 billion lb/yr by the early 1990s which is about the double of the production of 1987<sup><6></sup>. MTBE demand for methanol will triple to 1.2 billion gal in 1992, up from 400 million gal in 1989 and cause the global demand for methanol to grow more than 18% between 1989

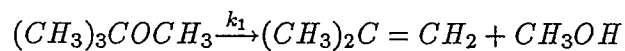
and 1992<sup><28></sup>.

There are several factors causing the demand of MTBE : the lead phasedown in gasoline in both the U. S. and in Europe, the failure of other nonlead oxygenates (e.g. ethanol...) to significantly improve octance ratings and therefore to serve as replacement for tetra ethyl lead in gasoline, plus the U. S. Environmental Protection Agency's restrictions on gasoline RVP (Reid Vapor Pressure) in order to decrease tropospheric ozone concentrations<sup><7></sup>.

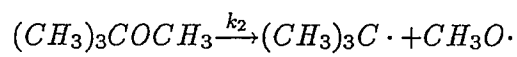
All the refiners in United States and most of those in Europe have accepted MTBE as an octane enhancer. It blends like a hydrocarbon and doesn't have the handling problems that alcohols do. It can also solve refiners' octane problems without requiring huge, additional capital investments. Many processes have been developed to reduce the cost of production<sup><8-13></sup> such as : a new process using sulfuric acid catalyst<sup><8></sup>, an adsorption process reducing control problems<sup><9></sup>, adding MTBE unit ahead of alkylation in refinery processing<sup><10></sup>, a bifunctional catalyst process<sup><11></sup> ... etc.

Detailed mechanisms of elementary reaction steps are valuable in the modeling of complex phenomena including ozone depletion, tropospheric air pollution, combustion and oxidation processes, and high-energy chemistry. The importance of kinetics in modeling chemical systems was emphasized by J. T. Herron and Stu Borman<sup><15></sup>. In

this study, a detailed kinetic mechanism for the high temperature combustion of MTBE is presented. This model based on fundamental thermodynamic and kinetic principles fits the data published by T. S. Norton and F. L. Dryer<sup><14></sup>. We determine rate constants for important reactions at 1 atm and temperature between 800 and 1200 K :



$$k_1 = 7.72 \times 10^{13} \exp(-29700/T) \text{ sec}^{-1}$$

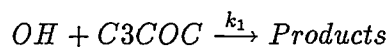


$$k_2 = 3.66 \times 10^{17} \exp(-39600/T) \text{ sec}^{-1}$$

## Chapter 2

# Previous Studies

T. J. Wallington<sup><16></sup>(1988) conducted a flash photolysis resonance fluorescence study on the kinetics of the hydroxyl radical (OH) reaction with MTBE over the temperature range 240 – 440 K at total pressures between 25 and 50 Torr. The Arrhenius expression for the overall rate constant was determined as follows :



$$k_1 = (5.1 \pm 1.6) \times 10^{-12} \exp[-(155 \pm 100)/T] \text{ cm}^3/\text{mole sec}$$

We note that this rate constant includes abstraction of both the methyl ether hydrogens and the primary methyl tert-butyl hydrogens.

There have been three previous experimental kinetic studies of rate constant determinations on the thermal decomposition kinetics of MTBE and they concluded that the reaction is a four-center molecular elimination.



Daly and Wentrup<sup><24></sup>(1968) reported that the decomposition reaction of MTBE is unimolecular and determined a rate constant, of  $10^{14.38} \exp(-30970/T) s^{-1}$  over the temperature range 706 to 768 K. Choo *et al.*<sup><25></sup>(1974) reported  $k = 10^{13.9} \exp(-29700/T) s^{-1}$  in a VLPP (Very Low-Pressure Pyrolysis) reactor at 890 – 1160 K, while Brocard and Baronnet<sup><26></sup>(1983) obtained  $k = 10^{14.0} \exp(-29960/T) s^{-1}$  in a Pyrex reactor at 725 to 761 K. These latter workers also found that the addition of propene or toluene did not modify the rate of formation of the major products, methanol and they concluded that a four-center unimolecular elimination path accounts for the homogeneous thermal decomposition of MTBE over their temperature and pressure ranges.

Other studies on the high temperature oxidation of methyl *tert*-butyl ether (MTBE) in argon diluent have been made by Dunphy and Simmie<sup><27></sup>(1989) in reflected shock waves over the temperature range 1024 to 1850 K and at a pressures of 3.5 bar. The mixture compositions varied widely, with equivalence ratios varying from 0.25 for a fuel-lean, through 1.0 for a stoichiometric, to 2.5 for a fuel-rich mix. Measurements of the ignition delay times, characterized by chemiluminescence and pressure rise, can be

concluded that the high temperature oxidation of MTBE is in essence that of methanol + iso-butene.

T. C. Norton and F. L. Dryer<sup><14></sup>(1990) presented the experimental results for flow reactor oxidation of MTBE at equivalence ratio 0.96, initial temperature of 1024 K and atmospheric pressure. Gas samples extracted at fifteen positions along the reactor duct centerline were quenched in the hot-water-cooled probe and stored at 70 °C for later gas chromatographic analysis. The purity of the MTBE was 97%.

The main products they observed were isobutene and methanol. A amount of 50 % MTBE was converted in a time of about 5 msec and 90% of conversion was achieved at about 40 msec. Isobutene and methanol were generated at up to 75% and 40% of initial MTBE concentration and decayed slowly compared to the MTBE decomposition rate. A increasing amount of carbon monoxide is produced. Methane and propene are observed at about 10% of MTBE initial concentration observed when MTBE conversion is 1.0. Other lower concentration products less than 10% of MTBE initial concentration such as  $CO_2$ ,  $C_2$ ,  $C_3$ , and  $C_5$ , are also produced.

Dryer and Norton describe the result of MTBE decay by the unimolecular elimination reaction only, which occurs through a four-center activated complex. They describe the final products observed as a result of a faster MTBE oxidation than either isobutene or methanol oxidations.

Although the identification of a series of elementary steps including production and loss of transient intermediates in the MTBE oxidation mechanism is unavailable, we have used known thermochemical kinetics and Transition State Theory with generic kinetic parameters to predict Arrhenius equations of the similar unknown reaction steps and build a mechanisms to explain the experimentally observed behavior. The results are presented in this thesis with the data of Norton and Dryer<sup>14</sup> used to validate our model.

## Chapter 3

# Theory

### 3.1 Transition-State and Collision Theory

#### 3.1.1 Transition-State Theory

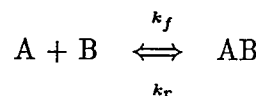
For many global reactions and particularly elementary reactions the rate expression can be written as a product of a temperature dependent term and a composition term.

$$\text{Rate} = -\frac{d[A]}{dt} = k \times [A] = A e^{-E_A/RT} [A]$$

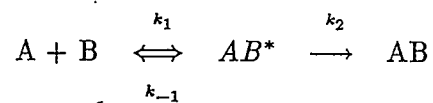
A detailed explanation for the transformation of reactants into products is given by the *transition-state theory* (TST) which was first proposed by Pelzer and Wigner<sup><18></sup> in 1932 and developed by Eyring, Polanyi, and their coworkers<sup><19></sup> during the 1930's — 1940's. The reactants combine to form an unstable intermediate called an *activated complex* which then decomposes spontaneously into products. TST assumes that an

equilibrium exists between the concentration of reactants and activated complex at all times and that the rate of decomposition of complex is the same for all reactions which is given by  $kT/h$ , where  $k$  is the *Boltzman constant* and  $h$  is the *Planck constant*.

Thus for the forward elementary reaction of a reversible reaction,



we have the following conceptual elementary scheme :



$$K^* = \frac{k_1}{k_{-1}} = \frac{[AB^*]}{[A] \times [B]} \quad (3.1)$$

$$(3.2)$$

$$k_2 = \frac{kT}{h} \quad (3.3)$$

The observed rate of the forward reaction is then,

$$\begin{aligned} R_{AB,forward} &= \text{Conc. of activated complex} \times \text{rate of decomposition of activated complex} \\ &= \frac{kT}{h} \times [AB^*] \\ &= \frac{kT}{h} \times K^* \times C_A \times C_B \end{aligned} \quad (3.4)$$

by expressing the equilibrium constant of activated complex in terms of the standard free energy,

$$\Delta G^* = \Delta H^* - T\Delta S^* = -RT \ln K^* \quad (3.5)$$

$$K^* = \exp(-\Delta G^*/RT) = \exp(-\Delta H^*/RT + \Delta S^*/R)$$

the rate becomes :

$$R_{AB,forward} = \frac{kT}{h} \times \exp(\Delta S^*/R) \times \exp(-\Delta H^*/RT) \times C_A \times C_B \quad (3.6)$$

Theoretically both  $\Delta S^*$  and  $\Delta H^*$  vary slowly with temperature. But, of the terms that make up the rate constant in Eqn. 3.5, the middle one,  $\exp(\Delta S^*/R)$ , is often so much less temperature-sensitive than the other two terms that we may take it to be constant. So for the forward reaction, and similarly for the reverse reaction of Eqn. 3.5, we have approximately :

$$\frac{k_f}{k_r} = \frac{T \exp(-\Delta H_f^*/RT)}{T \exp(-\Delta H_r^*/RT)} \quad (3.7)$$

where  $\Delta H_f^* - \Delta H_r^* = \Delta H_{rxn}$

### 3.1.2 Collision Theory

The collision rate of molecules in a gas can be found from the kinetic theory of gases described in standard undergraduate and advanced physical chemistry texts. For the bimolecular collisions of like molecules A we have

$$Z_{AA} = d_A^2 \times n_A^2 \times \frac{4kT}{M_A} = d_A^2 \times \frac{N^2}{10^6} \times \frac{4kT}{M_A} \times C_A^2 \quad (3.8)$$

- where  $d$  = diameter of molecule, cm  
 $M$  = mass of molecule, gm  
 $N$  = Avogadro's number  
 $C_A$  = concentration of A, mol/liter  
 $n_A$  = number of molecules of A per  $cm^3$   
 $k$  = Boltzmann constant

For bimolecular collisions of unlike molecules in mixture of A and B, kinetic theory gives :

$$Z_{AB} = \left(\frac{d_A + d_B}{2}\right)^2 \times \frac{N^2}{10^6} \times 8kT \times \left(\frac{1}{M_A} + \frac{1}{M_B}\right) \times C_A \times C_B \quad (3.9)$$

If every collision between reactant molecules results in the conversion of reactants into product, these expressions give the rate of bimolecular reaction. The actual rate is usually much lower than that predicted, and this indicates that only a small fraction of all collisions results in reaction. It suggests that only more energetic collisions, or more specifically, only those collisions that involve energies in excess of a given minimum energy  $E$  lead to reaction. From the *Maxwell Boltzman distribution law* of molecular energies the fraction of all bimolecular collisions that involve energies in excess of this minimum energy is given approximately by  $e^{(-E/RT)}$ , when  $E \gg RT$ . Since we are only considering energetic collisions, this assumption is reasonable. Thus, the rate of reaction is given by

$$-r_A = k \times C_A \times C_B$$

$$\begin{aligned}
 &= (\text{collision rate}) \times (\text{fraction of collisions involving energies in excess of } E) \\
 &= Z_{AB} \frac{10^3}{N} \exp(-E/RT) \\
 &= \left(\frac{d_A + d_B}{2}\right)^2 \times \frac{N}{10^3} \times 8kT \left(\frac{1}{M_A} + \frac{1}{M_B}\right) \exp(-E/RT) \times C_A \times C_B
 \end{aligned}$$

A similar expression can be found for the bimolecular collision between like molecules. For both, in fact for all bimolecular reaction, above equation shows that the temperature dependency of rate constant is given by

$$k \propto T^{1/2} e^{(-E/RT)}$$

### 3.1.3 Comparison of two theories

It is interesting to note the difference in approach between the Transition-State and Collision theories. Consider A and B colliding and forming an unstable intermediate which then decomposes into product, or



Collision theory views the rate to be governed by the number of energetic collisions between reactants. What happens to the unstable intermediate is of no concern. The theory simply assumes that this intermediate breaks down rapidly enough into products so as not to influence the rate of the overall process. Transition-state theory, on the other hand, views the reaction rate to be governed by the rate of decomposition of intermediate. The rate of formation of intermediate is assumed to be governed by

collision plus thermodynamics and it is present on equilibrium concentration at all times. Thus, collision theory views the first step to be slow and rate-controlling, where transition-state theory views the second step combined with the determination of complex concentration to be the rate controlling factors.

### 3.2 Prediction of Rate Constants Reaction by Unimolecular and Bimolecular QRRK Theory

The significant aspects of this thesis are the experimental results and the detailed chemical kinetic model, both of which are presented later on. The QRRK theory described below is very important to our model development research. A brief description of this theory from the article by *Westmoreland and Dean*<sup><20></sup> is paraphrased below and because of similarities we elect to treat it as a quotation.

The decomposition of a radical or molecule has a unimolecular, pressure-independent rate constant in the limit of high pressure, but as pressure is reduced the rate constant eventually falls off or decreases with pressure. In the low-pressure limit, it becomes directly proportional to the pressure.

Radical combination reactions or radical additions to unsaturated molecular are simply the reverse of decomposition, having the same fall-off behavior as the reverse reactions (microscopic reversibility). This is true for the specific reaction channel that

leads to formation of the collisionally stabilized adduct. The reason is that the adduct species has an initial energy distribution representing that of the thermal equilibrium levels of the reactants plus the energy of any new bond formed. It dissipates this via collision with surrounding gas molecules, just as for a species that is thermally decomposing. The stabilization ability of the surrounding gas molecules decreasing with increasing temperature.

It is however very important to note, but not so well recognized that additional products can be formed from the adduct produced by the the combination or addition reaction by this chemical activated pathway. "The initially formed adduct has a chemical energy distribution, different from a thermal energy distribution because the thermal energies of the reactant are augmented by chemical energy released by making the new bond. This chemical energy is initially the same as the energy barrier for redissociation of the collisionally stabilized adduct to the original adducts. If the energy in the chemical activation energy distribution extends above the barrier for a new dissociation ( or isomerization reaction pathway ) of the adduct, then that reaction pathway can also occur."

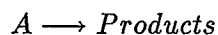
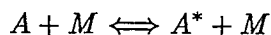
"Calculation of the bimolecular rate constant involves the concept that the fate of the chemically activated adduct is determined by competition among all the possible pathways : stabilization by collision, redissociation to reactants, or formation of new

products by dissociation or isomerization<sup><21></sup>.”

### 3.2.1 Unimolecular QRRK equation

”Dean<sup><21></sup> (1985) has presented equations for unimolecular and bimolecular rate constants based on the Quantum-RRK or QRRK unimolecular reaction theory of *Kassel* (1928), which treats the storage of excess energy relative to the ground state as quantized vibrational energy.”

In the simplest form of the theory, the assumption is made that the vibrations of the decomposing molecule can be represented by a single frequency  $\nu$ , usually a geometric mean  $\nu$  of the molecule's frequencies. Next, energy  $E$  initially activated of the complex and each barrier to reaction path relative to the ground state of the stabilized molecule is divided into  $E/h\nu$  vibrational quanta. For the total energy variable  $E$ , the symbol  $n$  is used; and for number of quanta to the energy barrier to reaction  $E_0$ , the quantized energy is  $m$  quanta; quantum level and the rate processes are illustrated in *Figure 3.1-a*. A very general scheme for unimolecular reaction is as follow :



Here  $M$  stands for the third body and only serves to raise the reacting molecule to its energized state  $A^*$  by collisional activation.

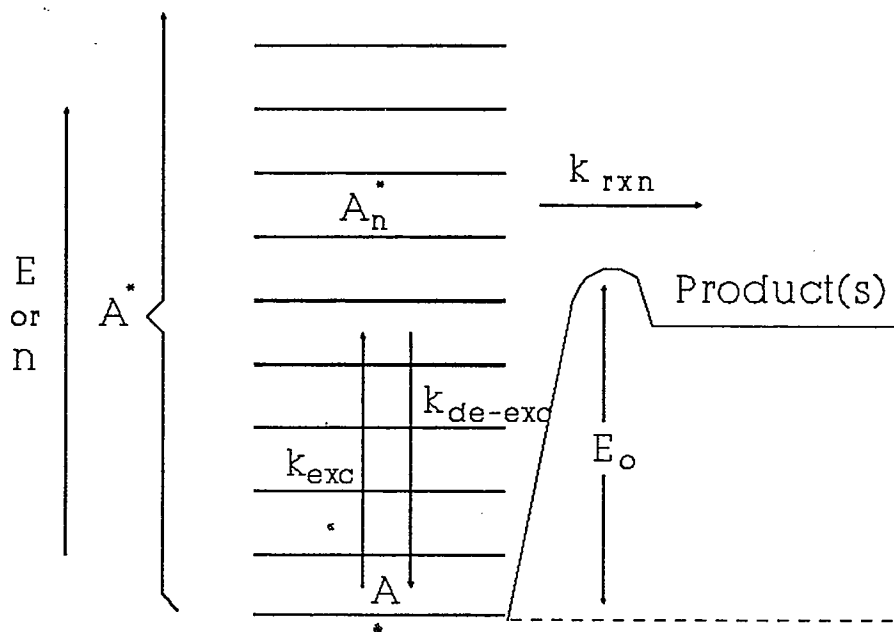


Figure 3.1-a. Unimolecular Reaction

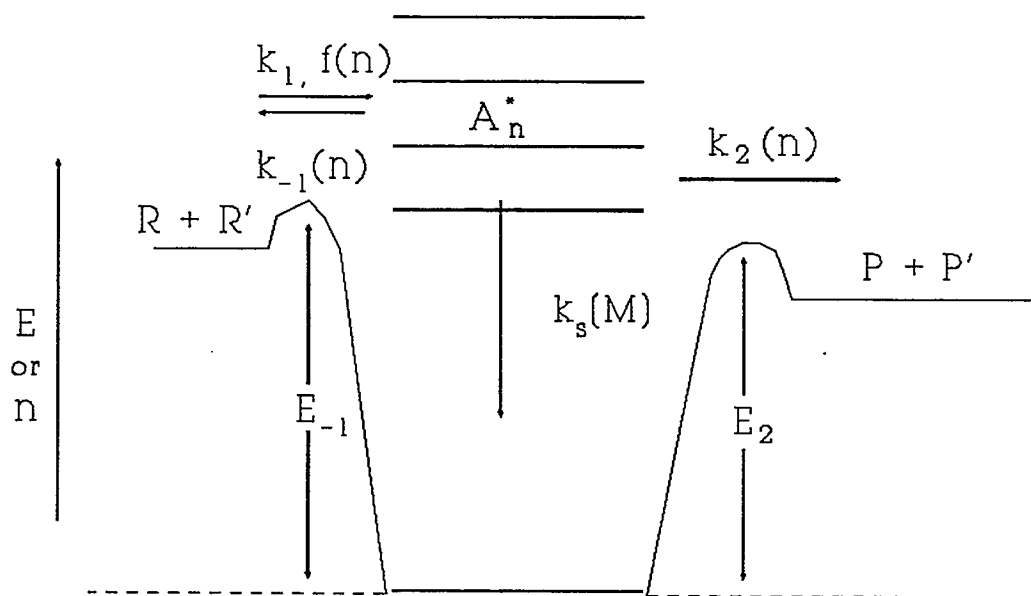


Figure 3.1-b. Bimolecular Reaction with Chemically Activated pathway

Figure 3.1 Energy Diagrams for Pressure-dependent Reactions

The apparent  $k_{uni}$  :

$$k_{uni} = \frac{1}{[A]} \times \frac{d[Products]}{dt} \quad (3.10)$$

then is evaluated by a sum over all energies, assuming pseudo-steady state for each energy level of  $A^*$  and collision excitation or deexcitation with rate constants  $k_{exc}$  and  $k_{de-exc}$  :

$$\begin{aligned} k_{uni} &= \frac{1}{[A]} \times k_{rxn}(E) [A^*(E)] \\ &= k_{rxn}(E) \times \frac{k_{de-exc}[M] \times K(E,T)}{k_{de-exc}[M] + k_{rxn}(E)} \end{aligned} \quad (3.11)$$

where  $K(E,T)$  is the thermal-energy distribution function ( $k_{exc}/k_{de-exc}$ ). Kassel assumed that if a molecule were excited to an energy  $E$ , then  $k_{rxn}(E)$  would be proportional to the probability that one of the  $s$  oscillators could have energy  $E_0$  or sufficient energy to cause reaction; that is,  $m$  or more of the  $n$  total quanta. The proportionality constant was shown to be  $A$ , the *Arrhenius preexponential factor* for dissociation of  $A$  in the high pressure limit, so the energy-dependent rate constant is :

$$k_{rxn}(E) = A \times \frac{n! \times (n - m + s - 1)!}{(n - m)! \times (n + s - 1)!} \quad (3.12)$$

"Likewise, Dean<sup><21></sup> derived the quantized thermal energy distribution  $K(E,T)$  to be :

$$K(E, T) = a^n (1 - a)^s \frac{(n + s - 1)!}{n! \times (s - 1)!} \quad (3.13)$$

where  $a = e^{-h\nu/kT}$ .

"In the present development, a collisional efficiency  $\beta$  has been applied to modify the traditional but incorrect strong-collision assumption that  $k_{de-exc} = Z[M]$ , where  $Z$  is collision frequency rate constant. The strong-collision assumption implied that any collision between  $A^*$  and  $M$  would have to remove all the excess energy from  $A^*$ ."

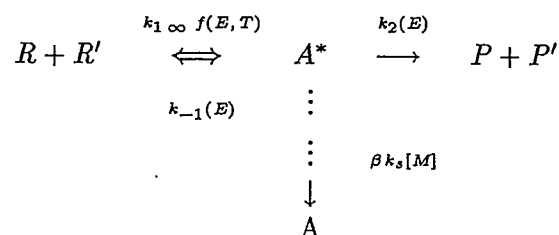
"Note that any species included as  $M$  would have to accommodate this energy content, regardless of its capacity for accepting the energy." Analyzing collisional energy transfer for master-equation methods, Troe (1977) fit most of the temperature dependence of  $\beta$  with the equation :

$$\frac{\beta}{1 - \beta^{1/2}} = \frac{-\Delta E_{coll}}{F(E) \times k \times T} \quad (3.14)$$

where  $E_{coll}$  is the average amount of energy transferred per collision and  $F(E)$  is a factor, weakly dependent on energy, that is related to the number of excited states. Over the temperature range of 300 - 2500  $K$  for a series of reactions ( Troe, 1977 );  $F(E) = 1.15$  was observed as a median value. The value of  $\beta$  depends on the specific third-body molecule  $M$  through the value of  $\Delta E_{coll}$ .

### 3.2.2 Bimolecular QRRK equation

"The bimolecular QRRK equation follows ( Dean, 1985 ) from unimolecular QRRK and the definition of the chemical activation distribution function." Consider recombination or addition to occur via the sequence :



Here R is a radical, R' is a radical (recombination reaction) or unsaturated molecule (addition reaction), A\* is the energized complex which can dissociate either back to products forward to other products or be collisionally stabilized,  $\beta$  is the temperature dependent collisional rate constant for stabilization.  $k_1$  is the high-pressure-limit rate constant for forming adduct and  $f(E,T)$  is the energy distribution for chemical activation :

$$f(E,T) = \frac{k_{-1} \infty f(E,T) K(E,T)}{\sum_{E_{crit}}^{\infty} k_{-1} K(E,T)} \quad (3.15)$$

where  $K(E,T)$  is the QRRK thermal distribution from Eqn. 3.16. Rate constant  $k_{-1}(E)$  and  $k_2(E)$  are calculated from the QRRK equation for  $k_{rxn}(E)$  using  $m_{-1}(E_{-1}/h\nu)$  and  $m_2(E_2/h\nu)$ , respectively. A typical energy diagram for these reaction is shown in Figure 3.1-b.

"To obtain the bimolecular rate constant for a particular channel, a pseudo-steady-state analysis is made as before. The rate constant for forming the stabilization product A from  $R + R'$  forming A\* :

$$k_{stab} = \frac{d[A]/dt}{[R][R']} = \beta k_s [M] \times \frac{k_1 f(E, T)}{\beta k_s [M] + k_{-1}(E) + k_2(E)} \quad (3.16)$$

and, for forming the decomposition products  $P + P'$  :

$$k_{dec} = \frac{d[Prod]/dt}{[R][R']} = k_2(E) \times \frac{k_1 f(E, T)}{\beta k_s [M] + k_{-1}(E) + k_2(E)} \quad (3.17)$$

If more decomposition channels are available, the  $k_{rxn}(E)$  for each channel is added in the denominator of Eqn. 3.15 and 3.16, and an equation in the form of Eqn. 3.16 is written for each additional channel, substituting the respective  $k_{rxn}(E)$  for  $k_2(E)$  as the multiplier term."

### 3.2.3 Low and High pressure limits

"The low-pressure and high-pressure limits for these channels may be derived from Eqn. 3.15 and 3.16. As pressure changes, the rate constants change because of the relative magnitudes of terms in the denominator,  $\beta k_s [M]$  vs.  $k_{-1}(E)$  and  $k_2(E)$ ."

"The low-pressure limit for stabilization is derived from Eqn. 3.15 to be

$$\lim_{M \rightarrow 0} k_{stab} = [M] \beta k_s \frac{k_1 f(E, T)}{k_{-1}(E) + k_2(E)} \quad (3.18)$$

sometimes written as  $[M]k_0$  (termolecular reaction), and the high-pressure limit reduces properly to  $k_1$ . At a given temperature, the fall-off curve for stabilization can be plotted as  $\log(k_{stab})$  vs.  $\log(P)$  or  $\log(M)$ ."

Note the presence of  $k_2(E)$  in Eqn. 3.17. "If chemically activated conversion of  $A^*$  is more rapid than decomposition to reactants ( $k_s(E) \gg k_{-1}(E)$ ), then Eqn. 3.17 shows that  $k_{0,stab}$  will be divided by  $k_2(E)$  rather than by  $k_{-1}(E)$ . Thus, ignoring the chemically activated pathway could give incorrect rate constants for "simple" addition."

"Similar analysis of Eqn. 3.16 implies that chemically activated decomposition back to reactants or to new products has a fall-off curve that is the opposite of stabilization, with a rate constant that is pressure-independent at low pressure and inversely proportional to pressure at high pressure. From Eqn. 3.16, the low-pressure limit for the chemically activated pathway to  $\mathcal{P}$  and  $\mathcal{P}'$  will be :

$$\lim_{M \rightarrow 0} k_{dec} = k_s \times \frac{k_2 f(E, T)}{k_{-1}(E) + k_2(E)} \quad (3.19)$$

and the high-pressure limit will be :

$$\lim_{M \rightarrow 0} k_{dec} = \frac{1}{[M]} \times \frac{k_1}{\beta k_s} \times k_2(E) \times f(E, T) \quad (3.20)$$

with an inverse pressure dependence. While this result goes against past intuition about low and high pressure limits, it is a natural consequence of physics when chemically activated reactions are recognized as possibilities. One commonly unrecognized consequence is that a reaction of the form  $A + B \rightarrow C + D$  with a rate constant measured to be pressure independent may be proceeding via activated complex formation with subsequent rapid decomposition of the complex to products ( $C + D$ ) before stabilization occurs."

## Chapter 4

# Results and Discussion

### 4.1 Important reactions

The detailed model of elementary reactions was constructed by determining the initial reactants and products and then considering plausible reactions of the products from the initial reaction. This process continued until the mechanism incorporated all the plausible and likely important reactions leading to the observed stable products; and accounted properly for experimental measurements of all the important intermediate species.

The initiation reactions are unimolecular decompositions of MTBE :

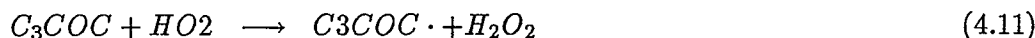




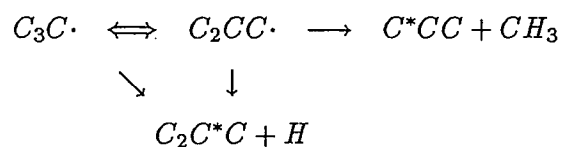
The channels involving loss of a H atom do not have to be taken into account due to the higher energy barrier of breaking the C-H bond comparing with C-O and C-C bonds. The A factors for this C-H bond is also lower further reducing the relative probability for these reactions. Reaction (4.1) is the dominant channels from the unimolecular QRRK analysis of DISSOC code when the temperature is lower than 1000 K. Reaction (4.2) becomes important or dominant at temperatures higher than 1000 K. This is consistent with the experimental observations of Norton et.al. < 14 >, that main products are isobutene and methanol.

Initial attack on MTBE by radical species present in the system is provided by H, O, OH, HO<sub>2</sub>, CH<sub>3</sub>O. and C<sub>3</sub>C.





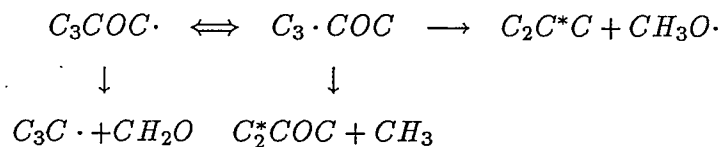
The thermal decompositions (Beta scissions) of  $C_3COC \cdot$ ,  $C_3 \cdot COC$ ,  $C_3C \cdot$ , and  $C_2C \cdot OC$  radicals and abstractions by other radicals are the most important reactions for the MTBE oxidation system. The elementary reaction rate parameters for abstraction reactions are based upon literature survey, thermodynamics and generic A factors with Evans Polanyi plots for Ea's. These radical decomposition rate constants are determined from the QRRK calculation as described in previous section.



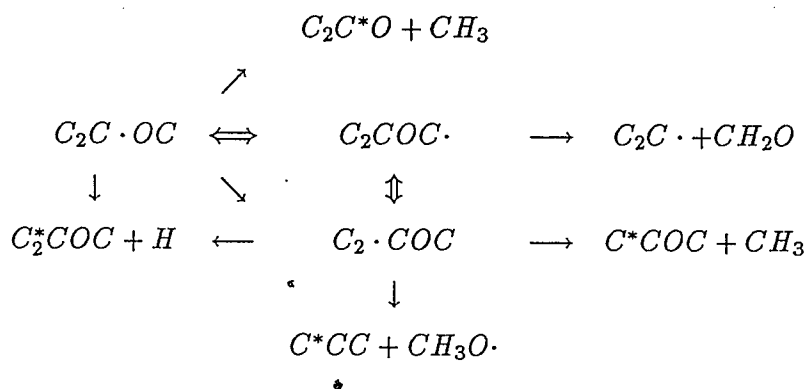
The above reactions can use two DISSOC calculations (unimolecular QRRK code), on *tert*-butyl radical and on *iso*-butyl radical decompositions, to obtain the apparent rate constants of reactions as a function of temperature and pressure. The dissociation reactions are :



The kinetic parameters for the unimolecular decomposition of  $C_3COC\cdot$  and  $C_3\cdot$   $COC$  reactions can also be obtained by DISSOC's calculations.



The corresponding radicals of *iso*-propyl methyl ether are also the important species in MTBE oxidation system. The following reactions contribute to the formation of acetone and propene.



In such a complex system, several combinations of unimolecular and bimolecular QRRK's need to be evaluated to obtain the rate constants for each step. Here, a combination of three DISSOC calculations was utilized.





$CH_3$  and  $CH_3O \cdot$  abstract other species to form  $CH_4$  and  $CH_3OH$  or recombine with  $O$ ,  $H$ , and  $OH$ .  $CH_3$  also reacts with  $O_2$  to  $CH_3OO \cdot$  and  $CH_2 \cdot OOH$ . Higher temperatures or oxygen rich conditions accelerate radical generation reactions and the formation of  $CO$  and  $CO_2$ . Dean<sup><21></sup> and Tsao's<sup><30></sup> kinetic data on hydrocarbon oxidation reactions are adopted for hydrocarbon pyrolysis and oxidation and  $H_2$ - $O_2$ - $CO$  system respectively.

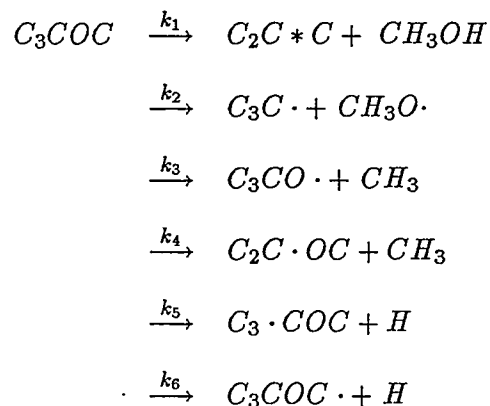
## 4.2 Important Dissociation Reactions

The decomposition of the energized radical and molecular complexes was modeled using the QRRK calculations. The details of the bimolecular QRRK method are presented in the theory section. Its application to a number of chemically activated reaction systems have been previously discussed<sup><20>,<21></sup>.

Energized complex/QRRK theory as presented by *Westmoreland* and *Dean*<sup><21></sup> is used for modeling of radical addition reactions. This computer code has been modified by *Ritter* and *Bozzelli*<sup><22></sup> to use *gamma function* instead of factorials. The QRRK computer code was used to determine the energy dependent rate constant for all reactions of the energized complexes formed by combination of radicals or by radical addition to an unsaturated and calculates rate constants as function of both temperature and pressure. The use of this formalism is important in determination of accurate rate constants needed for input to the mechanism, specifically in choice of the important reaction paths as a function of temperature and pressure. This is also applied to accurate product distribution predictions from dissociation of the activated complex.

A QRRK analysis of the chemically activated system, using generic estimates or literature values for high pressure rate constants and species thermodynamic properties for the enthalpies of reaction, yields thermodynamically and kinetically plausible apparent rate constants. The input rate parameters used in these calculations and results from the calculation are summarized in APPENDIX A. The following sections are the applications of unimolecular QRRK.

#### 4.2.1 Unimolecular Dissociation of $C_3COC$



The MTBE dissociation reaction is the most important reaction in the both of the MTBE pyrolysis and oxidation reaction system. The energy level diagram and input parameters for the chemical activation calculations are shown in Fig 4.1 and Appendix B.1 respectively.

The calculation results shown in Fig 4.2, 4.3, 4.4 and 4.5 indicate that the dominant channels are the dissociations to  $(C_2C * C + CH_3OH)$  and  $(C_3C \cdot + CH_3O \cdot)$ . The apparent rate constants of both reactions are consistent with their high pressure limits when the temperature is lower than 800 K and pressure higher than 0.001 atm. The ratio of  $k_1/k_2$  shown in Table 4.1, Fig 4.6 and 4.7 as a function of temperature and pressure, is about 60 at 800 K and increases as temperature decreases.

The unimolecular elimination of channel (1) is dominant when the temperature lower than  $\sim 900$  K. This is consistent with why Daly *et al.*<sup><24></sup> and Choo *et al.*<sup><25></sup>

concluded that the decomposition reaction of MTBE is a four-center molecular elimination at temperatures  $\sim 700$  K.

The effect of temperature on the falloff behavior of dissociation reactions is dramatic. Fig 4.2 illustrates that increasing the temperature from 800 to 1200 K for ( $C_3COC \rightarrow C_3C \cdot + CH_3O \cdot$ ) shifts the falloff curve by 4 orders of magnitude toward higher pressure. The result indicates the dramatic differences between application of the present approach and use of the assumption that the dissociation is always at the high pressure limit. The difference between the actual dissociation rate constant and the high pressure limit increases when the temperature is above 1000 K at the atmospheric pressure.

The falloff curves for three channels are very consistent. The detailed apparent rate constants are shown in Appendix B.1. The data provide accurate kinetic parameters of the specific temperature and pressures for this high temperature reaction system.

Figure 4.1 Energy Diagram of C<sub>3</sub>COC

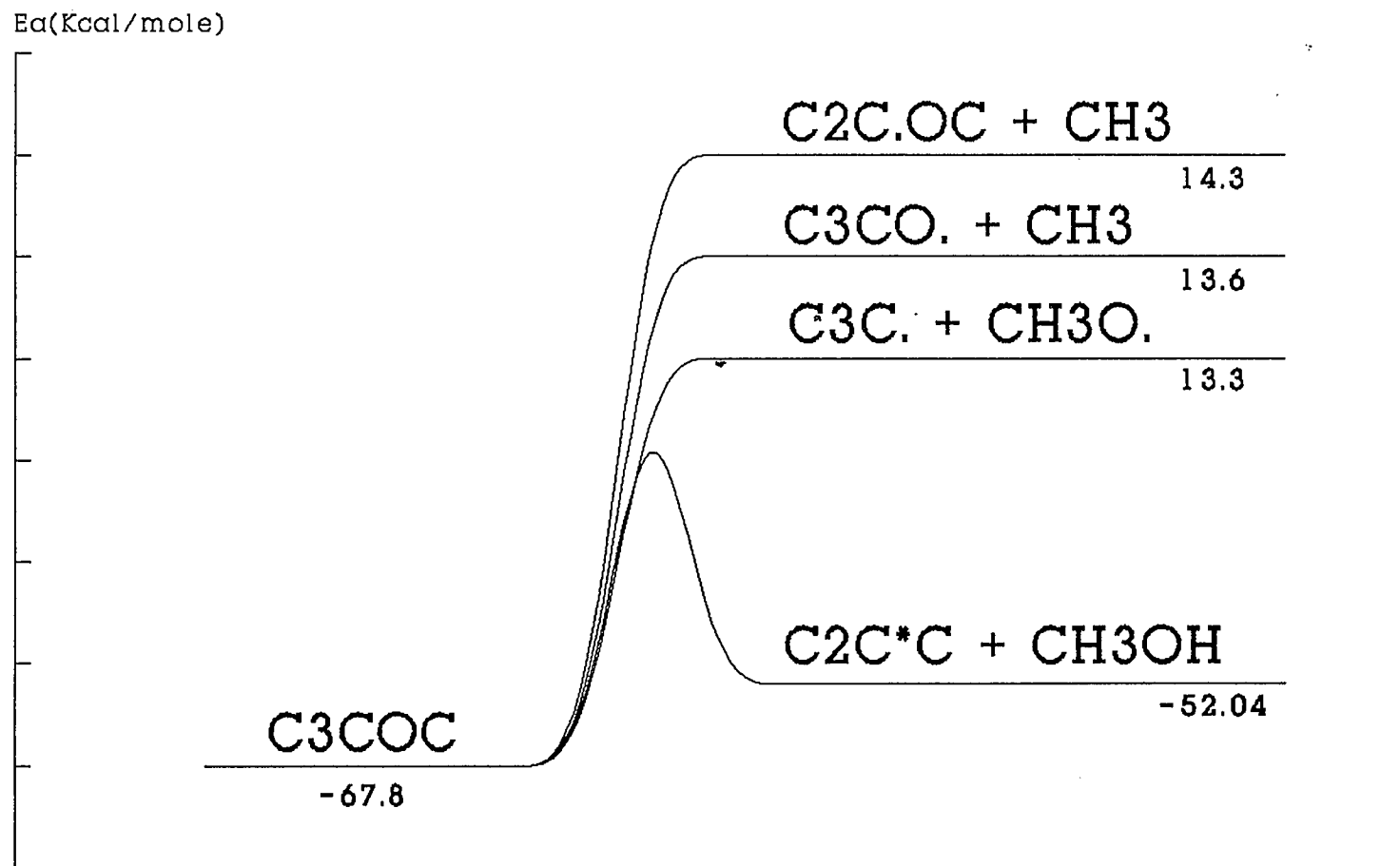


Figure 4.2  $k_1/k_2$  as a Function of Pressure

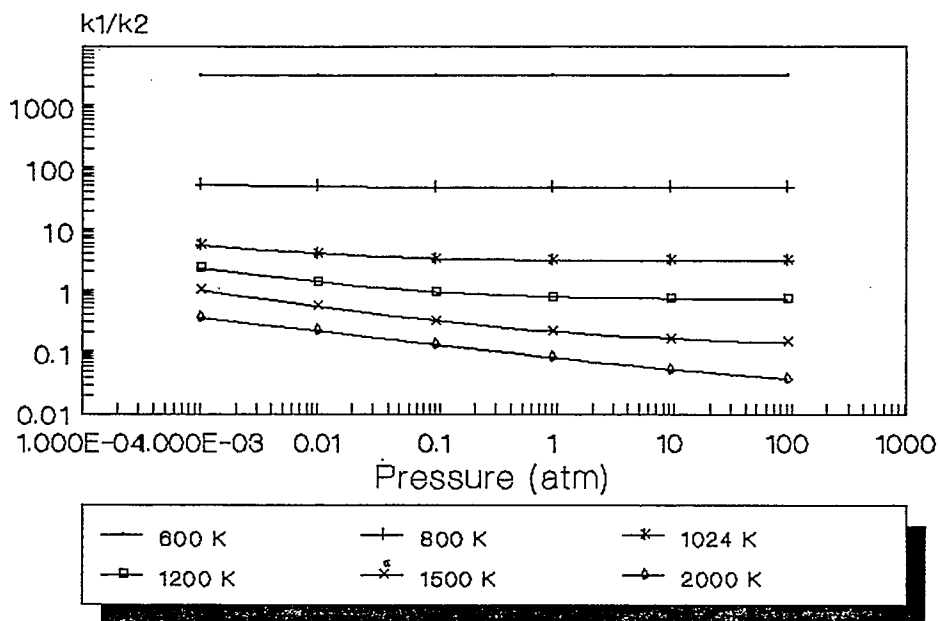


Figure 4.3  $k_1/k_2$  as a Function of Temperature

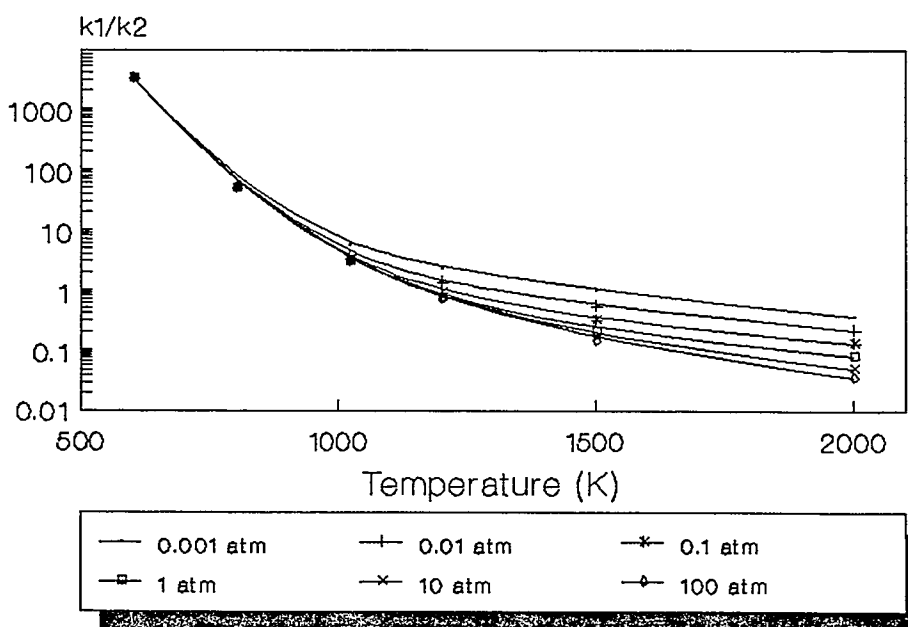


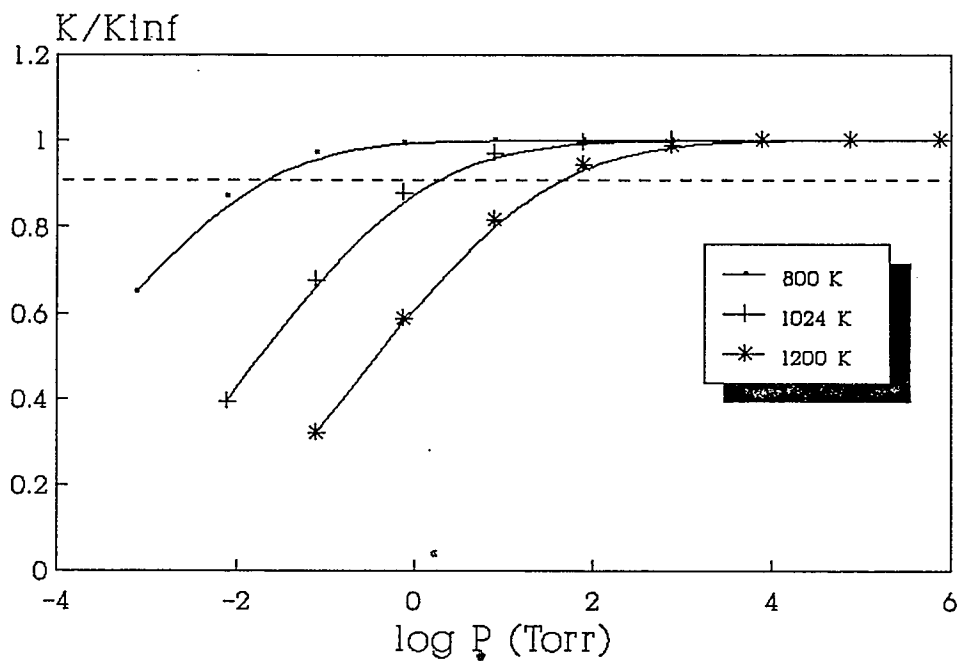
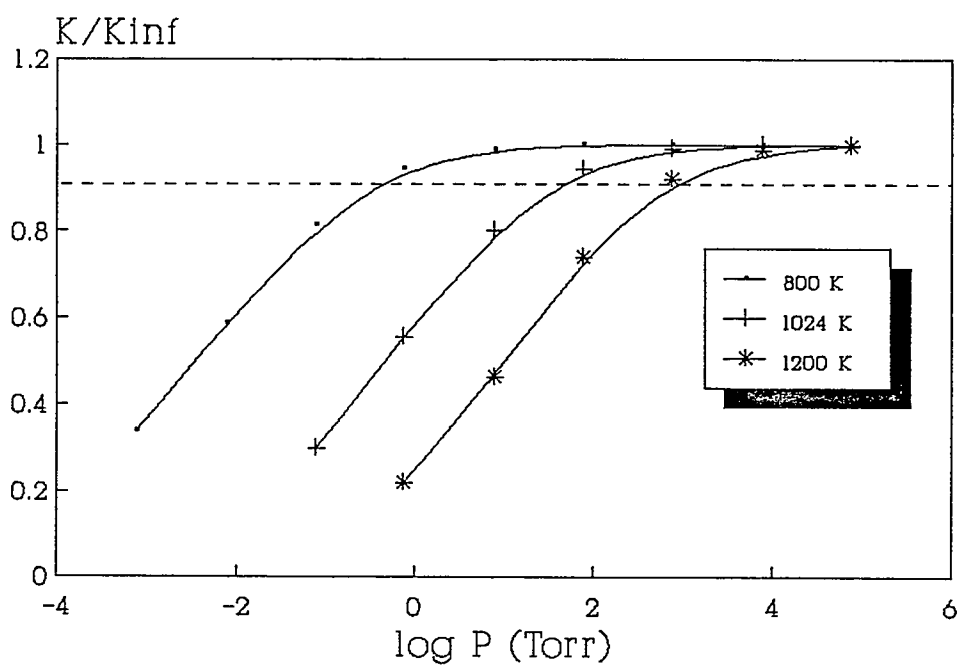
Figure 4.4 Fall-Off Curve of  $C_3CO \rightarrow C_2C + CH_3OH$ Figure 4.5 Fall-Off Curve of  $C_3CO \rightarrow C_3C + CH_3O$ 

Figure 4.6 Predicted Rate Constants for C<sub>3</sub>COC Dissociation as a Function of Pressure at 1024 K with N<sub>2</sub> as Bath Gas

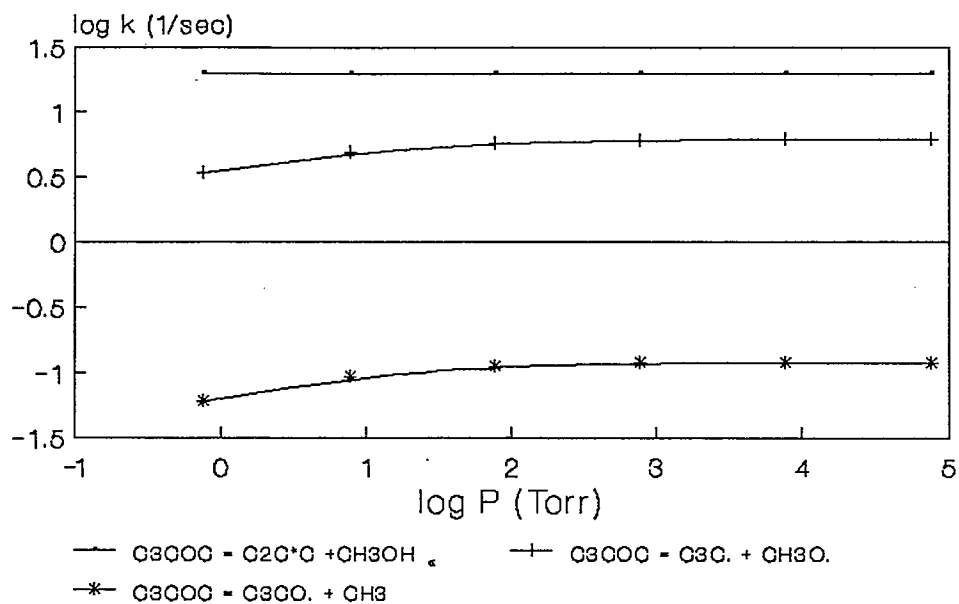
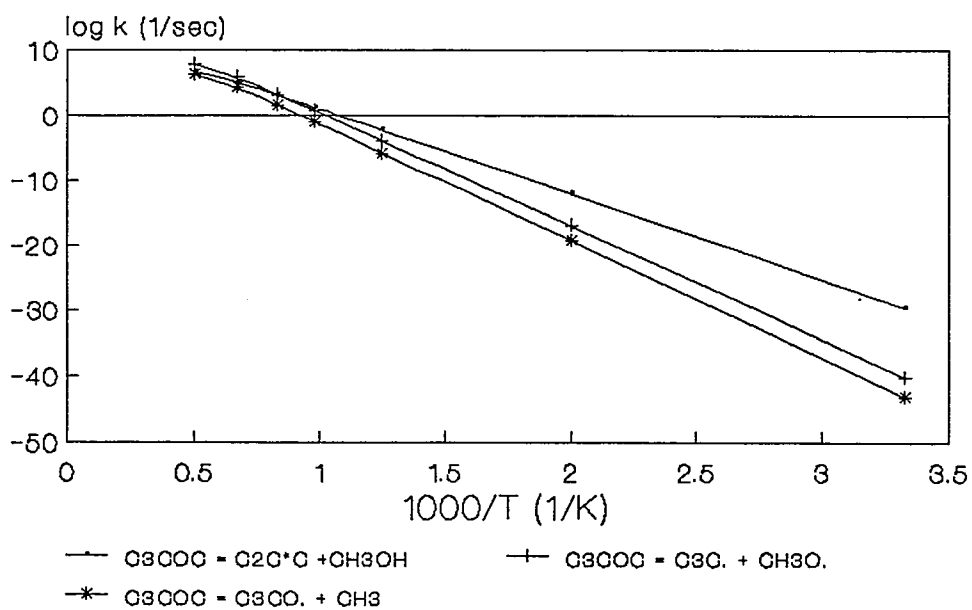
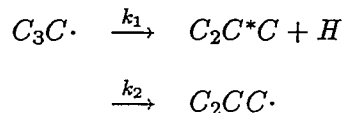


Figure 4.7 Predicted Rate Constants for C<sub>3</sub>COC Dissociation as a Function of Temperature at 1 atm with N<sub>2</sub> as Bath Gas



### 4.2.2 Unimolecular Dissociation of $C_3C\cdot$

The energy diagram and calculation results, are shown in Fig 4.8, 4.9 and 4.10 for the  $C_3C\cdot$  unimolecular dissociation reaction system.



There are two channels for  $C_3C\cdot$  to decompose through breaking the C-H bond to form *iso*-butene and intramolecular isomerization, 3 member cyclic intermediate, to  $C_2CC\cdot$ . Reaction (1) is about ten times faster than reaction (2) for pressures above 1.0 atm, and more than ten times faster for pressures below 1.0 atm. That is due to high energy barrier and tight transition state (low A factor) to isomerization, although reaction (2) goes to a lower final energy level.

Detailed output results for  $C_3C\cdot$  unimolecular reaction are presented in Appendix B.2 which list the kinetic parameters for the temperature and pressure ranges of 800 to 1200 K and 7.6 to 760 Torr.

# Figure 4.8 Energy Diagram of C3C.

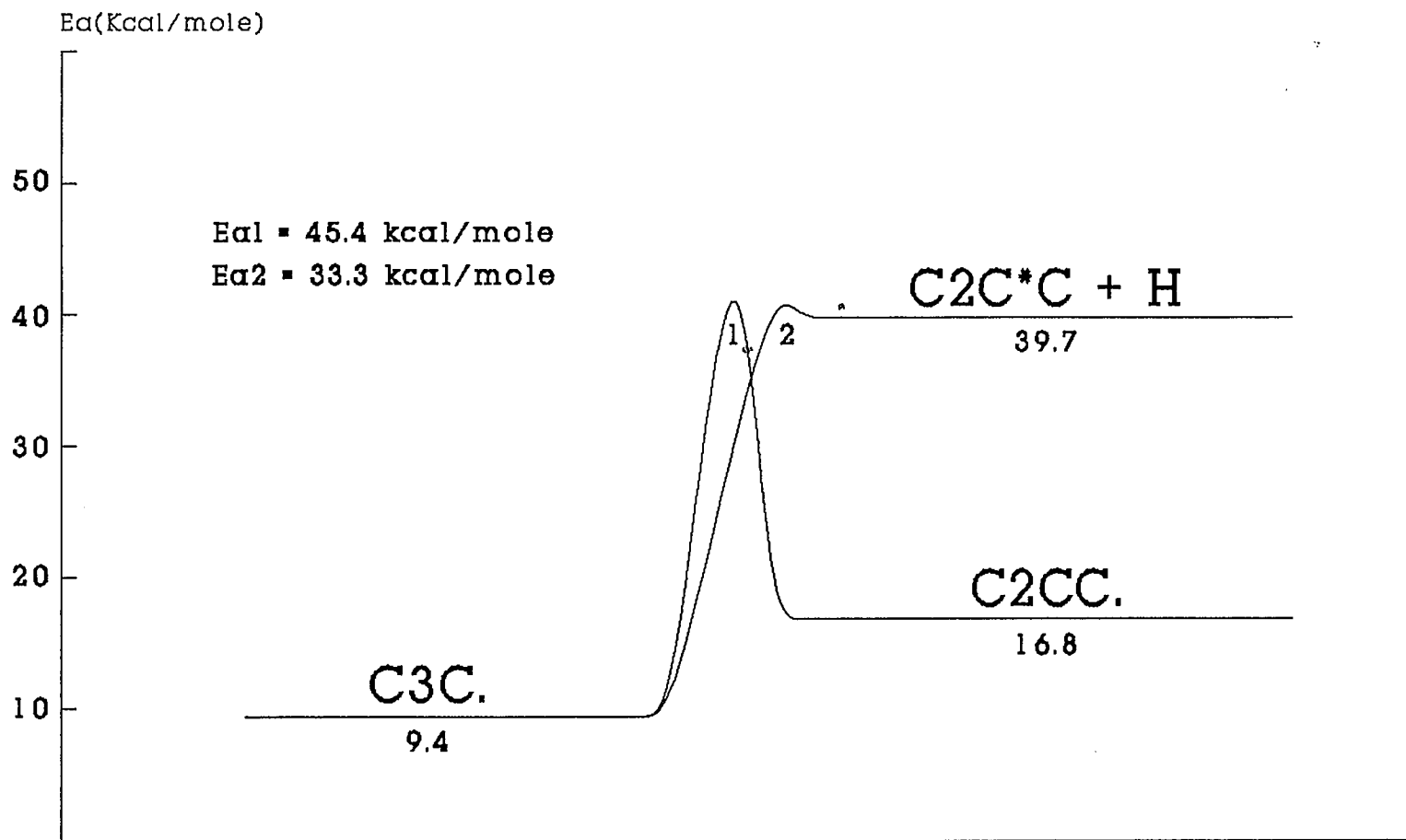


Figure 4.9 Predicted Rate Constants for C<sub>3</sub>C. Dissociation as a Function of Temperature at 1 atm with N<sub>2</sub> as Bath Gas

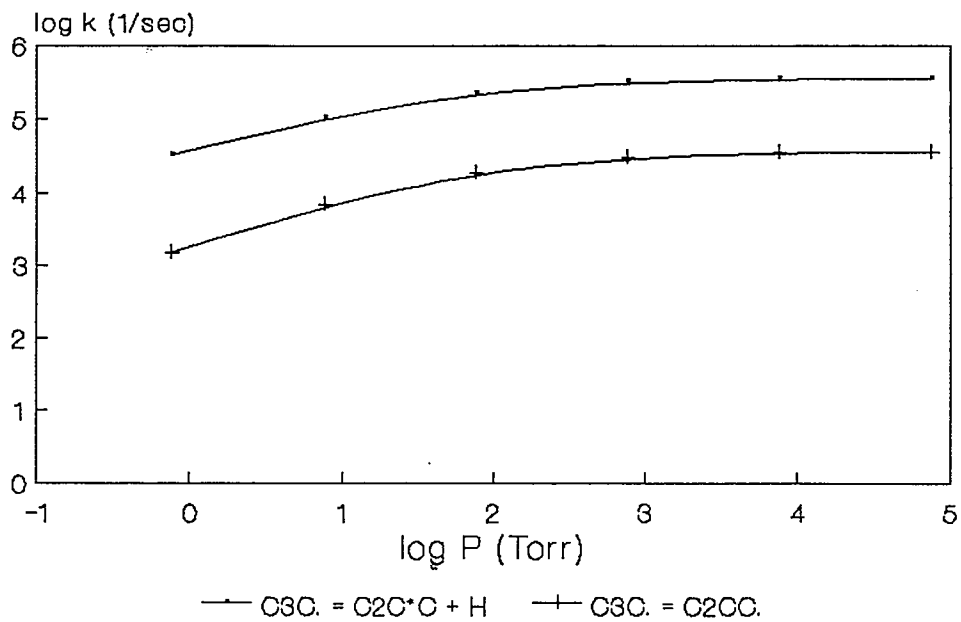
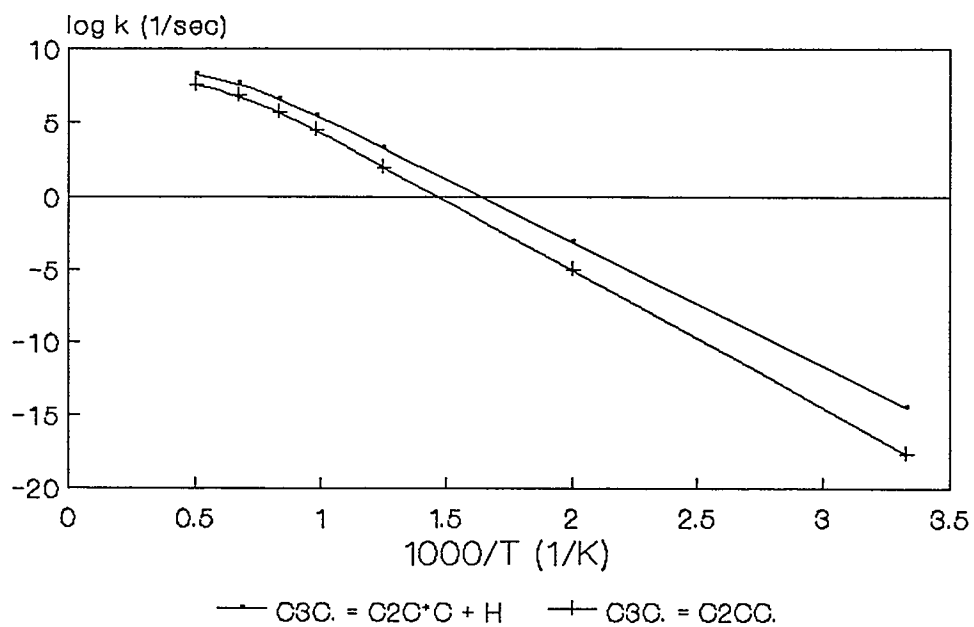
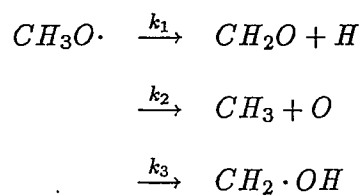


Figure 4.10 Predicted Rate Constants for C<sub>3</sub>C. Dissociation as a Function of Temperature at 1 atm with N<sub>2</sub> as Bath Gas



### 4.2.3 Unimolecular Dissociation of $CH_3O\cdot$

The energy diagram and calculation results, are shown in Fig 4.11, 4.12 and 4.13 for the  $CH_3O\cdot$  unimolecular dissociation reaction system.



Reaction (1) is the dominant channel. Detailed output results for  $CH_3O\cdot$  unimolecular reaction are presented in Appendix B.3 which list the kinetic parameters for the temperature and pressure ranges of 800 to 1200 K and 7.6 to 760 Torr.

Figure 4.11 Energy Diagram of CH<sub>3</sub>O.

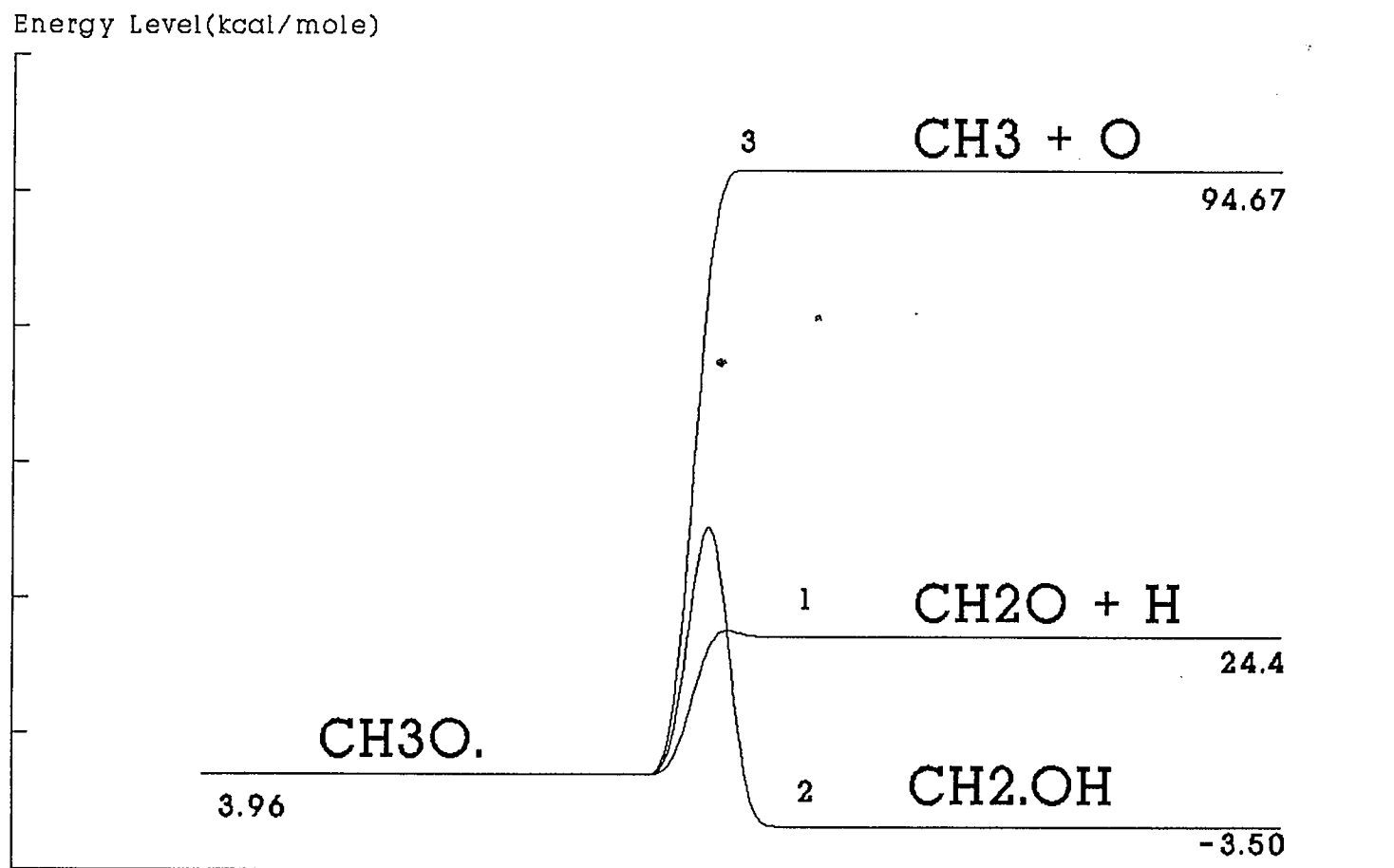


Figure 4.12 Predicted Rate Constants for CH<sub>3</sub>O. Dissociation as a Function of Pressure at 1024 K with N<sub>2</sub> as Bath Gas

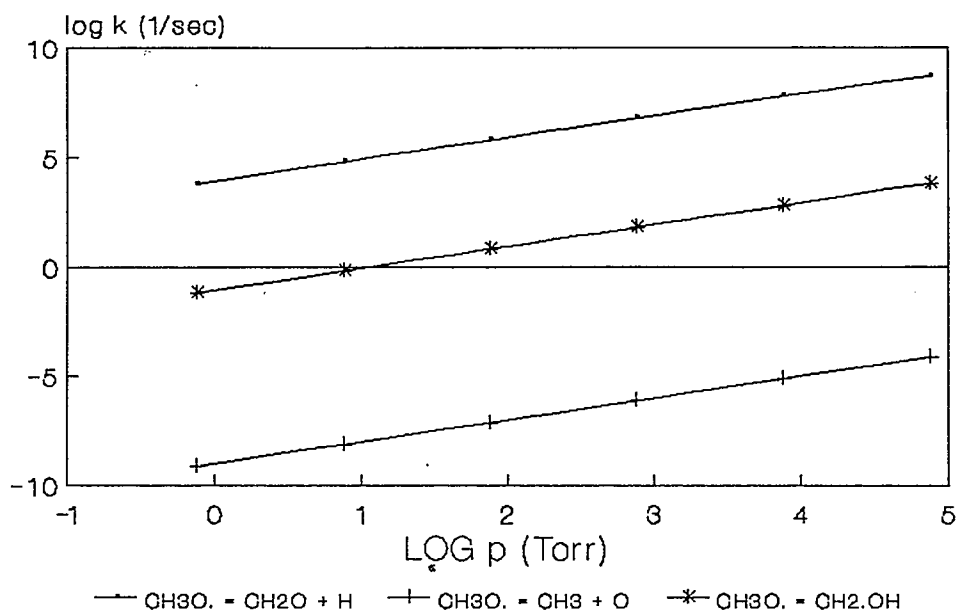
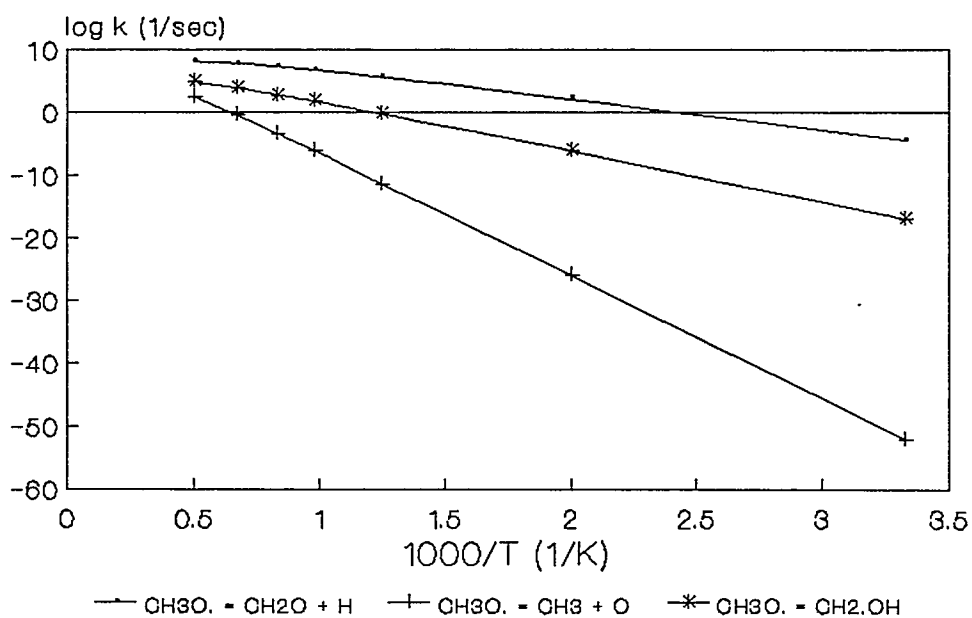
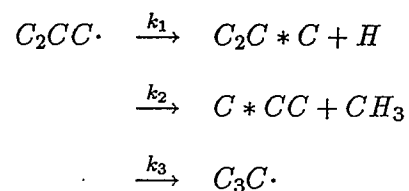


Figure 4.13 Predicted Rate Constants for CH<sub>3</sub>O. Dissociation as a Function of Temperature at 1 atm with N<sub>2</sub> as Bath Gas



#### 4.2.4 Unimolecular Dissociation of $C_2CC\cdot$

The energy diagram and calculation results, are shown in Fig 4.14, 4.15 and 4.16 for the  $C_2CC\cdot$  unimolecular dissociation reaction system.



The rate constants of these reactions are below their high pressure limit values at atmospheric pressure and 1000 K. Reaction (2) is the dominant channel. Detailed output results for  $C_2CC\cdot$  unimolecular reaction are presented in Appendix B.4 which list the kinetic parameters for the temperature and pressure ranges of 800 to 1200 K and 7.6 to 760 Torr.

Figure 4.14 Energy Diagram of C2CC.

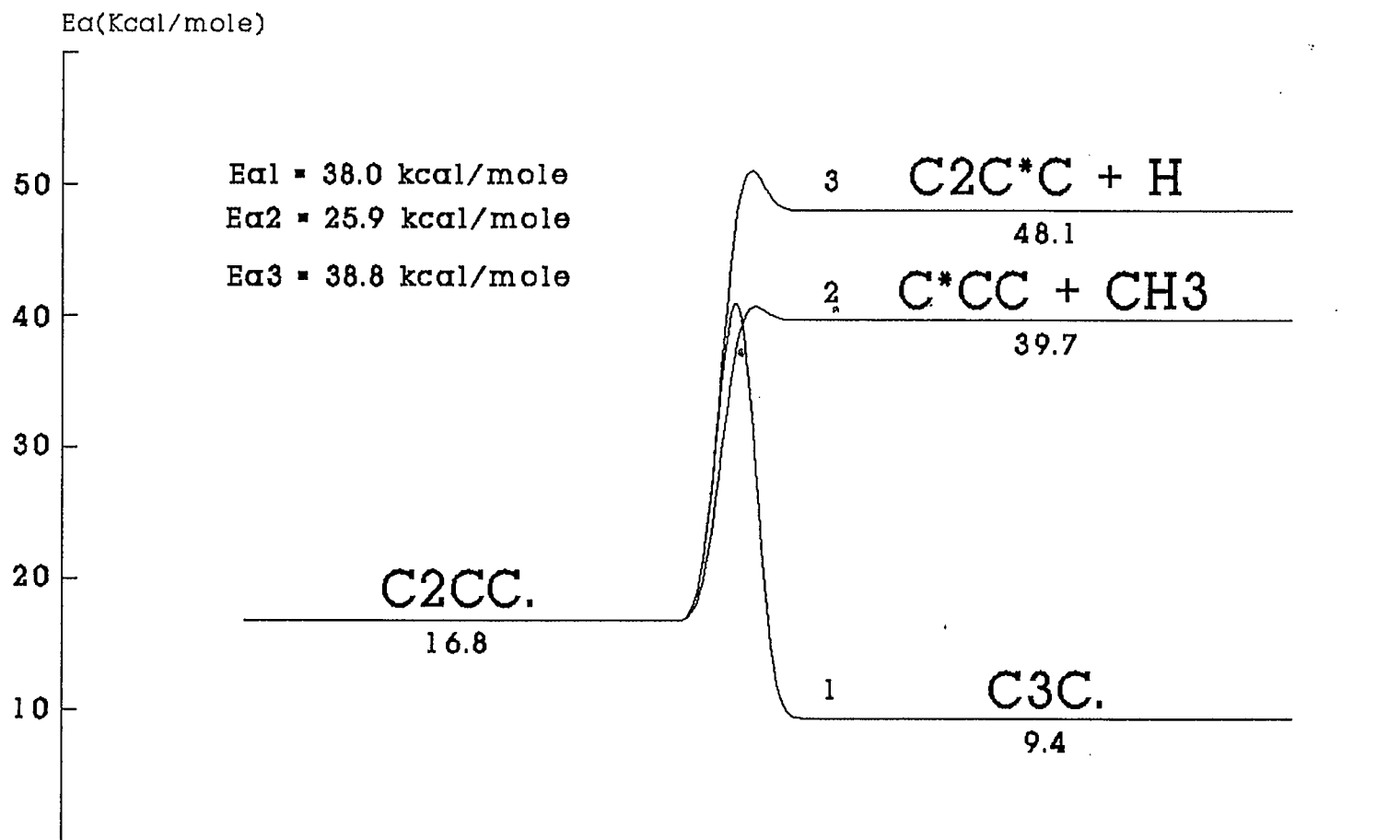


Figure 4.15 Predicted Rate Constants for C<sub>2</sub>CC<sub>2</sub> Dissociation as a Function of Pressure at 1024 K with N<sub>2</sub> as Bath Gas

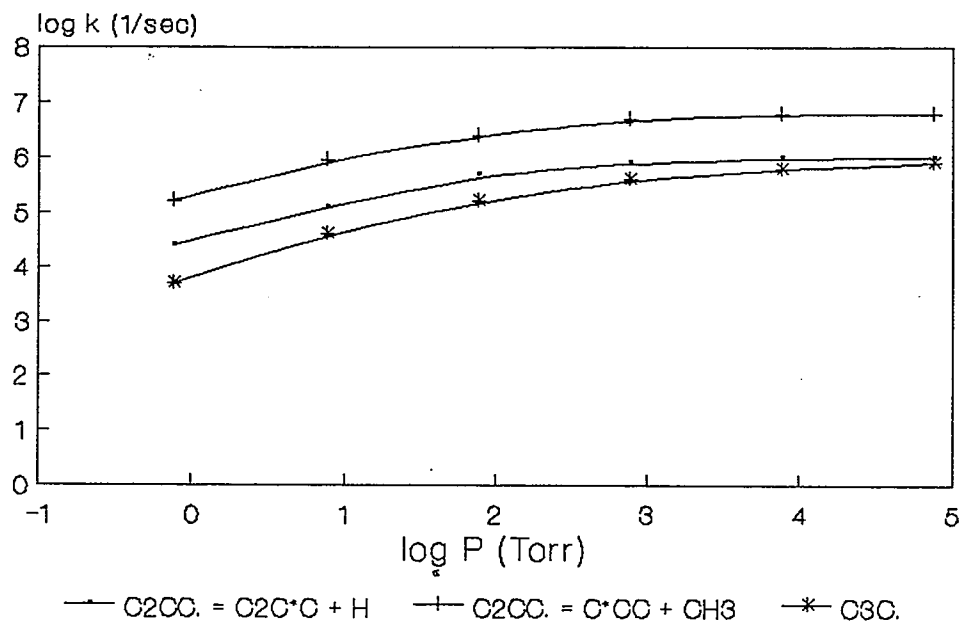
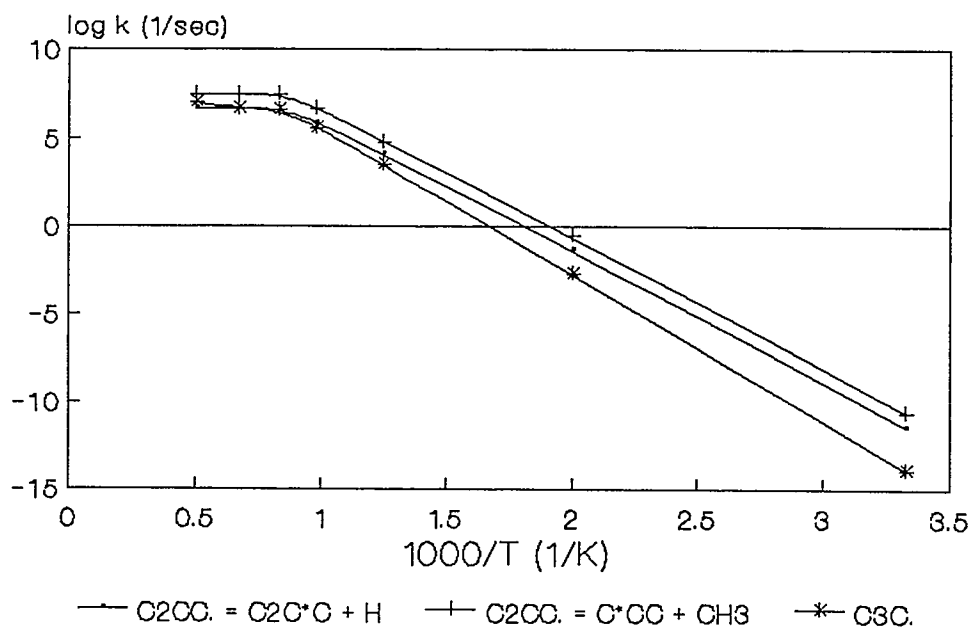
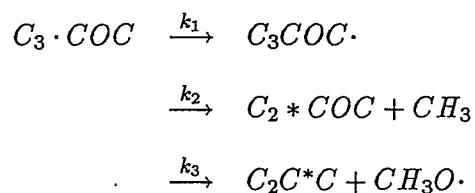


Figure 4.16 Predicted Rate Constants for C<sub>2</sub>CC<sub>2</sub> Dissociation as a Function of Temperature at 1 atm with N<sub>2</sub> as Bath Gas



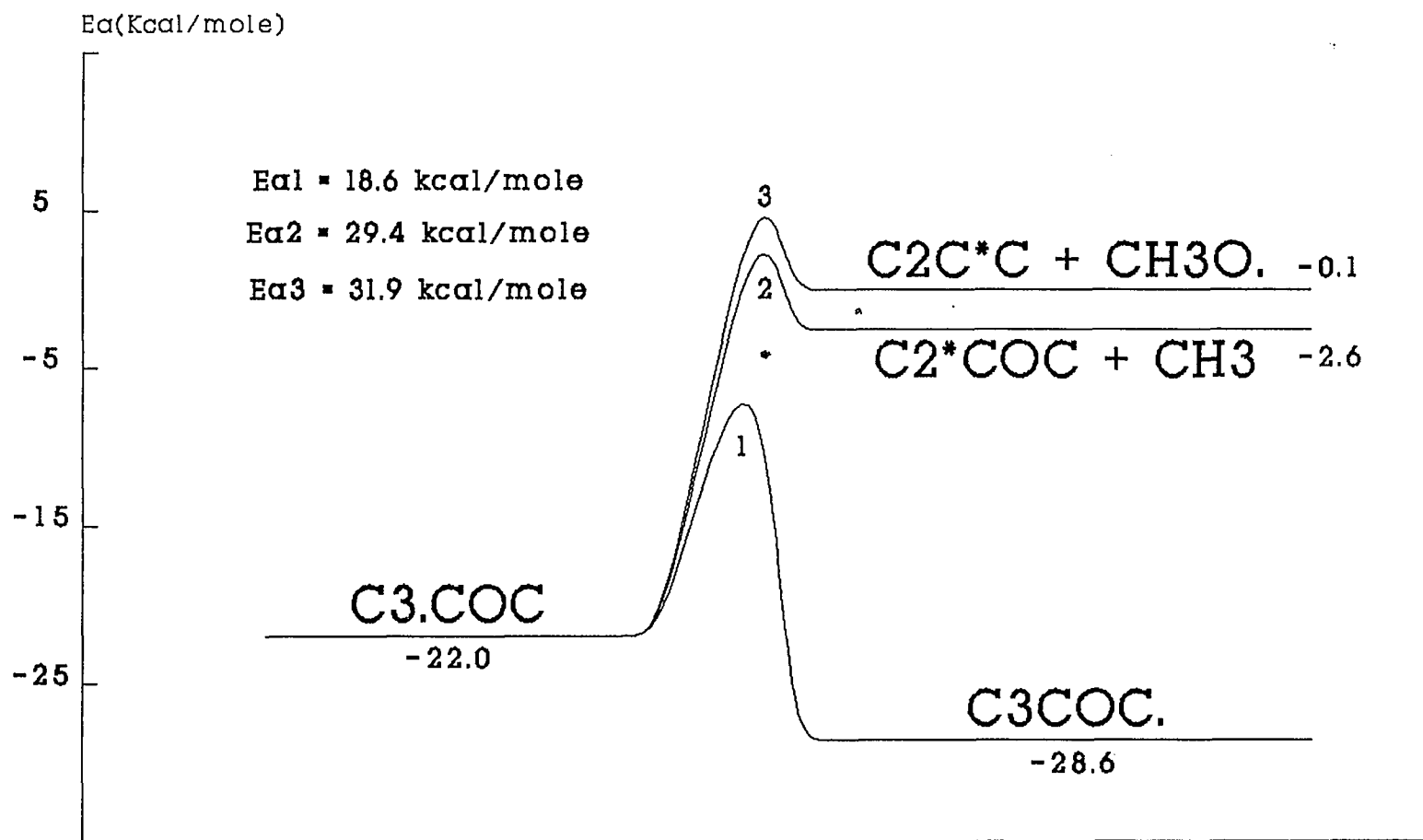
#### 4.2.5 Unimolecular Dissociation of $C_3 \cdot COC$

The energy diagram and calculation results, are shown in Fig 4.17, 4.18 and 4.19 for the  $C_3 \cdot COC$  unimolecular dissociation reaction system.

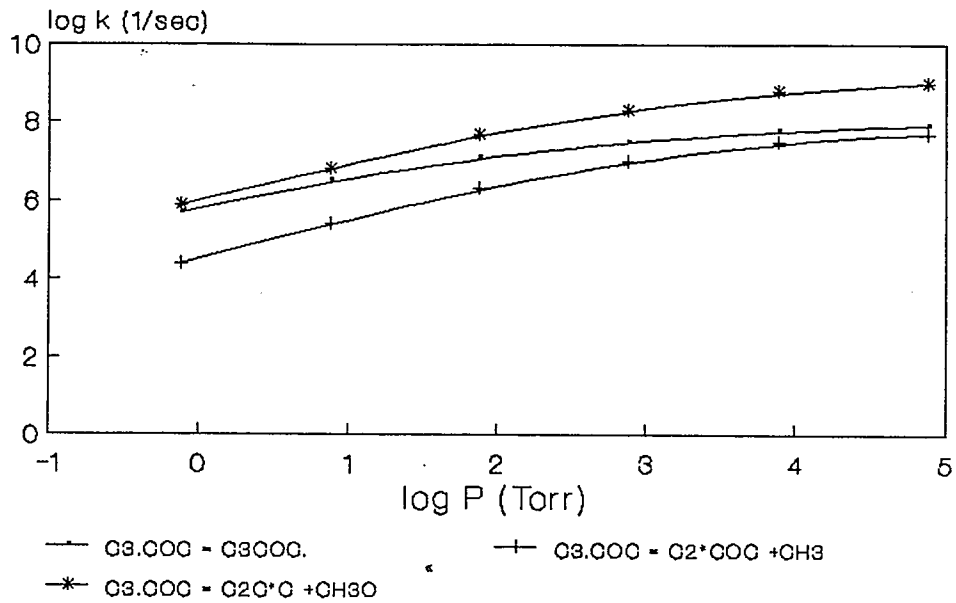


The rate constants of these reactions are below their high pressure limit at atmospheric pressure and 1000 K. Reaction (3) of  $C_3 \cdot COC$  dissociation to  $C_2C^*C$  (iso-butene) and  $CH_3O \cdot$  is the dominant channel. Reaction (1) which undergoes a intramolecular isomerization, 5 member cyclic intermediate, to  $C_3COC \cdot$ , is about ten times slower than reaction (3) due to the high energy barrier, although it goes to a lower final energy level. Reaction (2) is also limited by a lower A factor than Reaction (3) even though it is slightly more thermodynamically favorable.

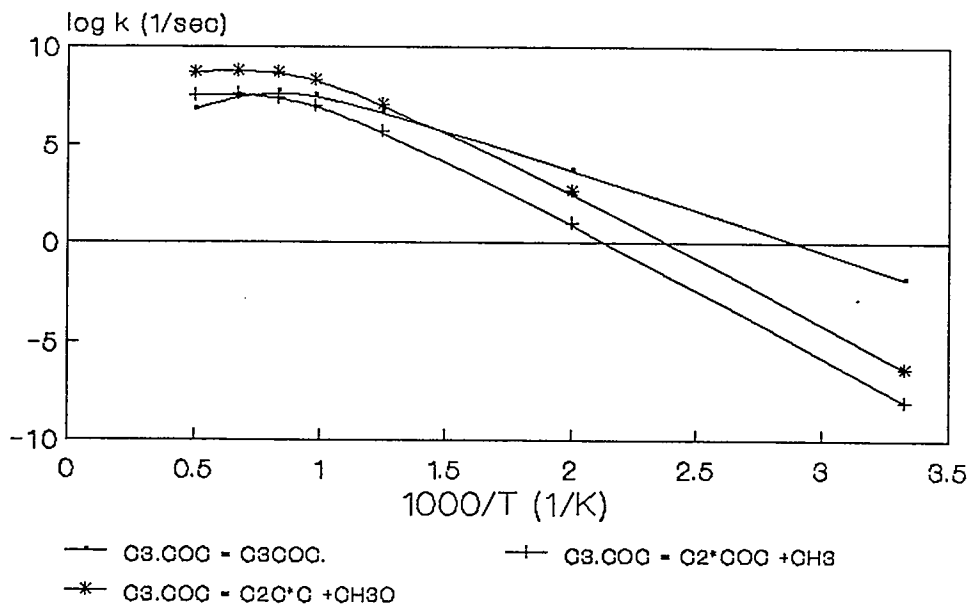
Detailed output results for  $C_3 \cdot COC$  unimolecular reaction are presented in Appendix B.5 which list the kinetic parameters for the temperature and pressure ranges of 800 to 1200 K and 7.6 to 760 Torr.

Figure 4.17 Energy Diagram of C<sub>3</sub>COC

**Figure 4.18 Predicted Rate Constants for C<sub>3</sub>COC Dissociation as a Function of Pressure at 1024 K with N<sub>2</sub> as Bath Gas**

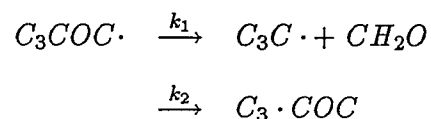


**Figure 4.19 Predicted Rate Constants for C<sub>3</sub>COC Dissociation as a Function of Temperature at 1 atm with N<sub>2</sub> as Bath Gas**



#### 4.2.6 Unimolecular Dissociation of $C_3COC\cdot$

The energy diagram and calculation results, are shown in Fig 4.20, 4.21 and 4.22 for the  $C_3\cdot COC$  unimolecular dissociation reaction system.



The rate constants of these reactions are below their high pressure limit at atmospheric pressure and 1000 K. Reaction (1) is dominant. Reaction (2) which undergoes a intramolecular isomerization, 5 member cyclic intermediate, to  $C_3COC\cdot$ , does not occur due to the high energy barrier.

Detailed output results for  $C_3COC\cdot$  unimolecular reaction are presented in Appendix B.6 which list the kinetic parameters for the temperature and pressure ranges of 800 to 1200 K and 7.6 to 760 Torr.

Figure 4.20 Energy Diagram of C<sub>3</sub>COC.

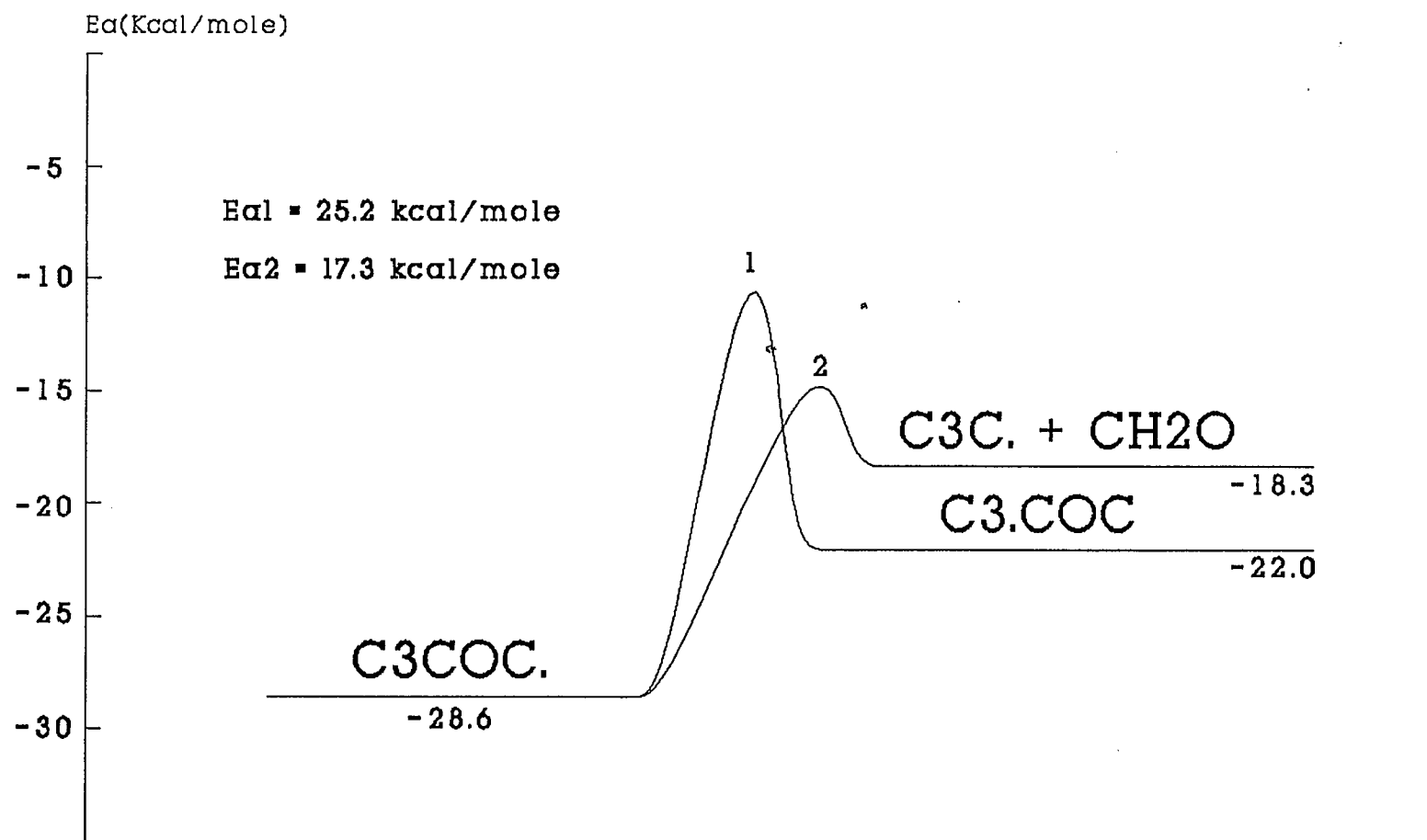


**Figure 4.21** Predicted Rate Constants for C<sub>3</sub>COG. Dissociation as a Function of Pressure at 1024 K with N<sub>2</sub> as Bath Gas

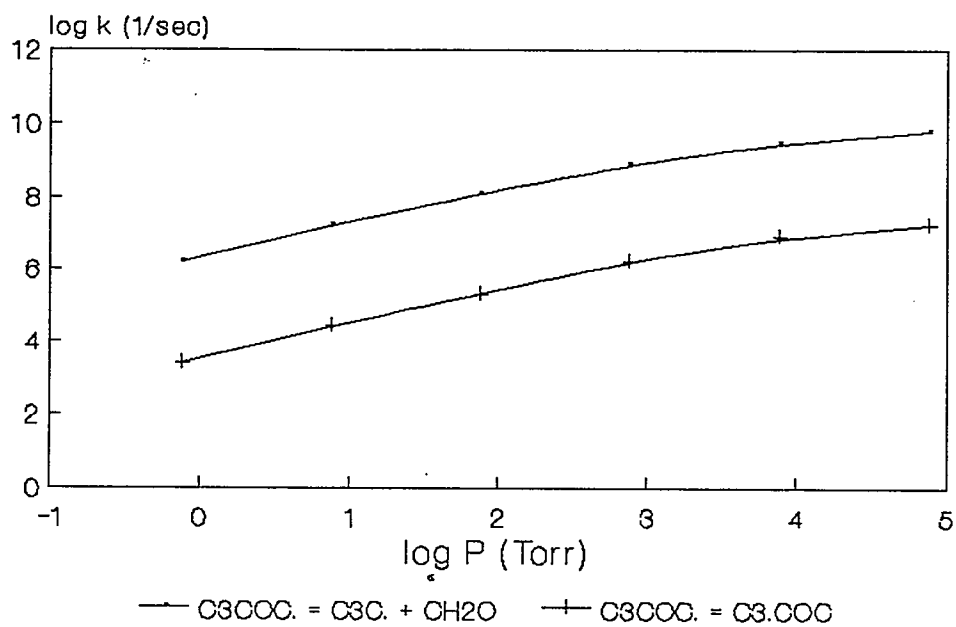
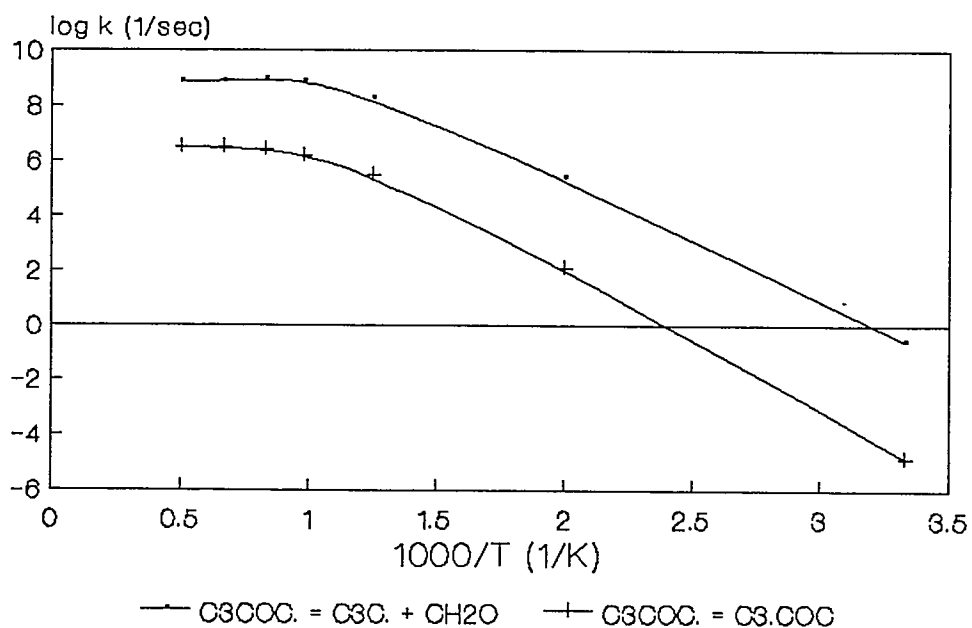
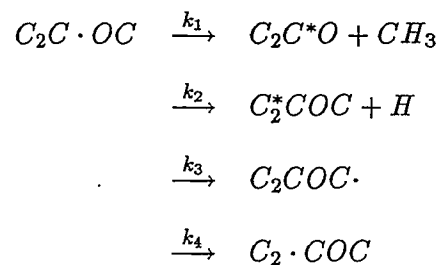


**Figure 4.22** Predicted Rate Constants for C<sub>3</sub>COG. Dissociation as a Function of Temperature at 1 atm with N<sub>2</sub> as Bath Gas



#### 4.2.7 Unimolecular Dissociation of $C_2C \cdot OC$

The energy diagram and calculation results, are shown in Fig 4.23, 4.24 and 4.25 for the  $C_2C \cdot OC$  unimolecular dissociation reaction system.



The rate constants of these reactions are below their high pressure limit at atmospheric pressure and 1000 K. Reaction (1) is dominant. Reaction (2), (3), and (4) are not important due to the high energy barriers.

Detailed output results for  $C_2C \cdot OC$  unimolecular reaction are presented in Appendix B.7 which list the kinetic parameters for the temperature and pressure ranges of 800 to 1200 K and 7.6 to 760 Torr.

# Figure 4.23 Energy Diagram of C2C.OC

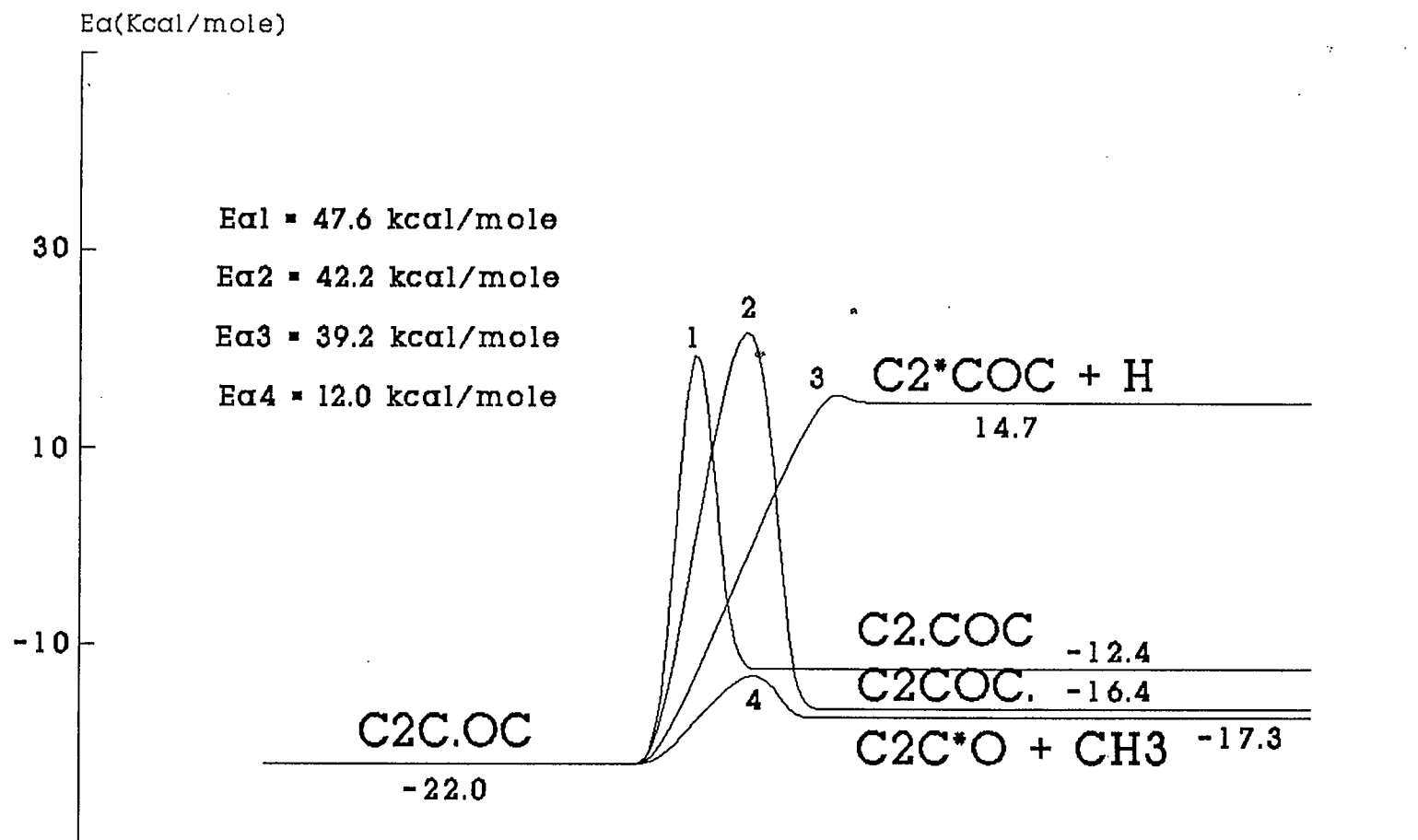


**Figure 4.24 Predicted Rate Constants for C<sub>2</sub>C<sub>2</sub>O<sub>2</sub> Dissociation as a Function of Pressure at 1024 K with N<sub>2</sub> as Bath Gas**

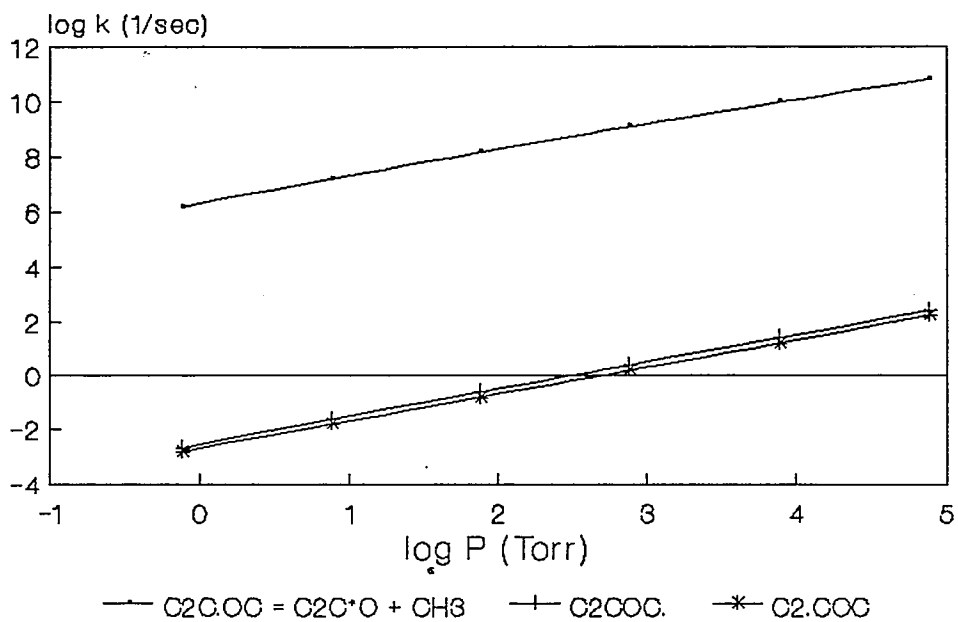
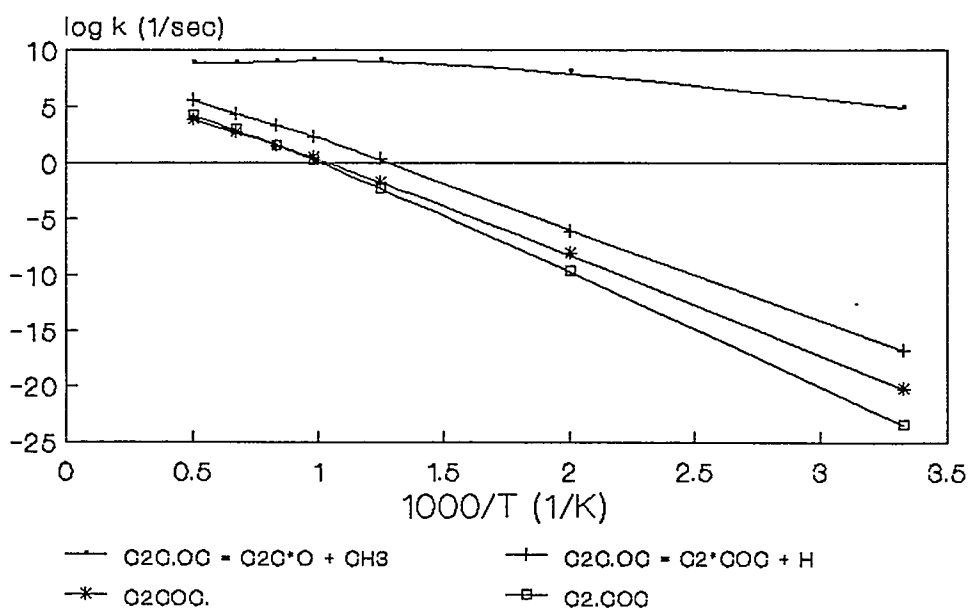
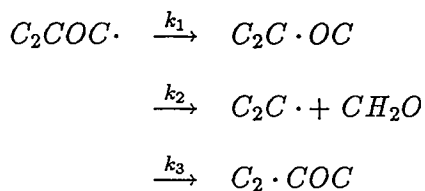


**Figure 4.25 Predicted Rate Constants for C<sub>2</sub>C<sub>2</sub>O<sub>2</sub> Dissociation as a Function of Temperature at 1 atm with N<sub>2</sub> as Bath Gas**



#### 4.2.8 Unimolecular Dissociation of $C_2COC\cdot$

The energy diagram and calculation results, are shown in Fig 4.26, 4.27 and 4.28 for the  $C_2COC\cdot$  unimolecular dissociation reaction system.



The rate constants of these reactions are below their high pressure limit at atmospheric pressure and 1000 K. Reaction (2) is dominant. Reaction (1) and (3) which undergo the intramolecular isomerizations, 4 and 5 member cyclic intermediate respectively, to  $C_2C\cdot OC$  and  $C_2\cdot COC$ , do not occur to a significant degree due to the high energy barriers, although they go to a lower final energy levels.

Detailed output results for  $C_2COC\cdot$  unimolecular reaction are presented in Appendix B.8 which list the kinetic parameters for the temperature and pressure ranges of 800 to 1200 K and 7.6 to 760 Torr.

Figure 4.26 Energy Diagram of C<sub>2</sub>COC.

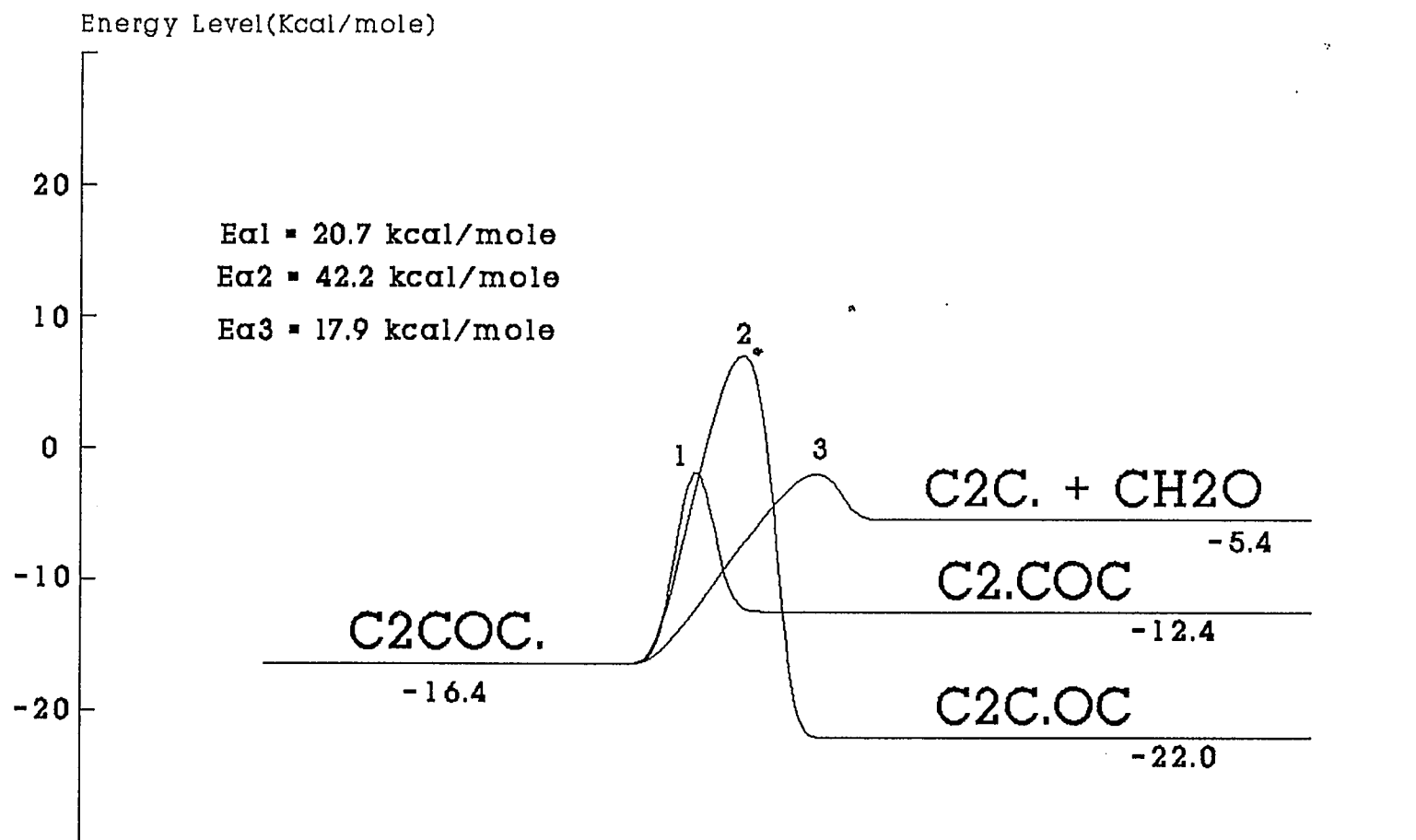


Figure 4.27 Predicted Rate Constants for C<sub>2</sub>OOC. Dissociation as a Function of Pressure at 1024 K with N<sub>2</sub> as Bath Gas

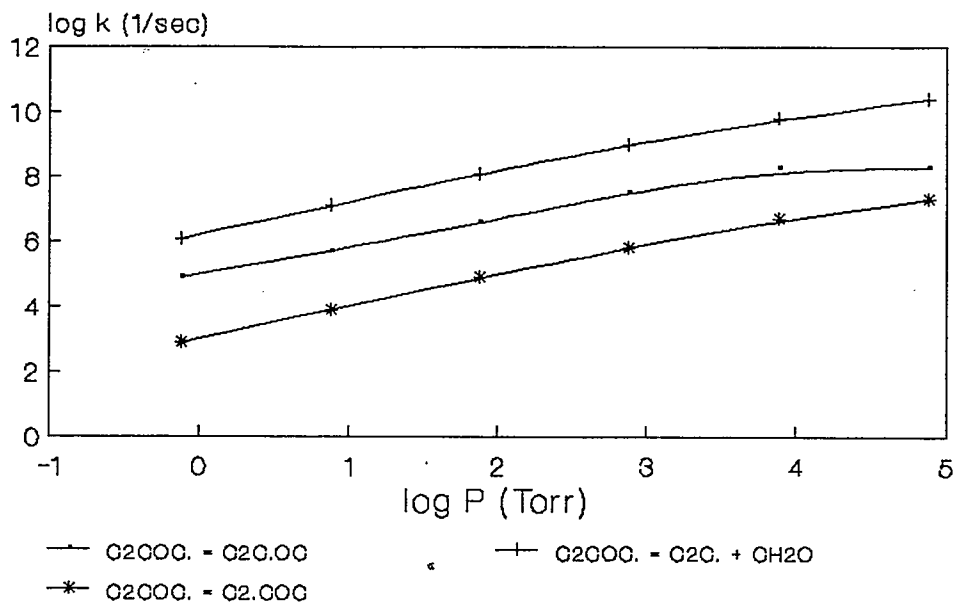
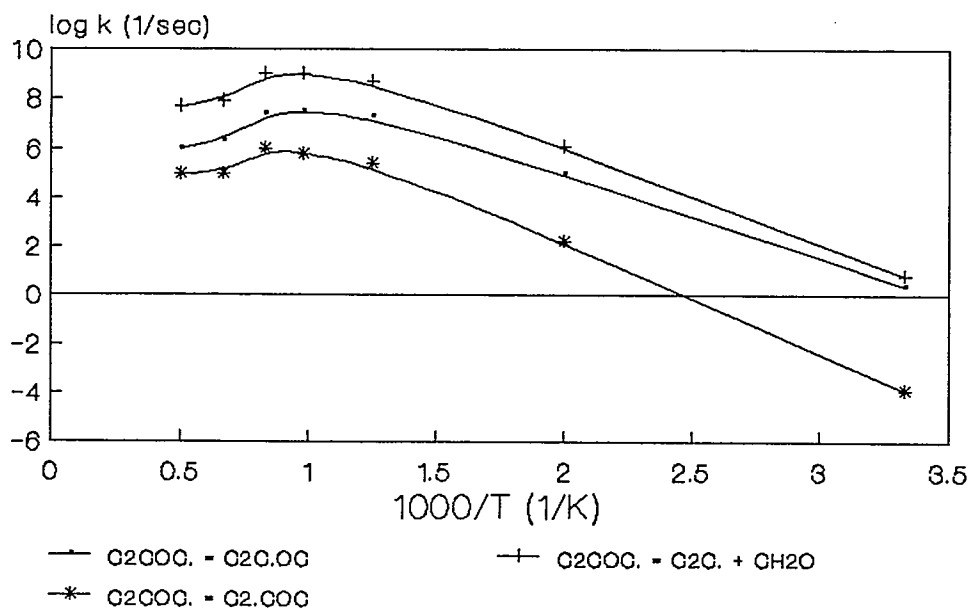
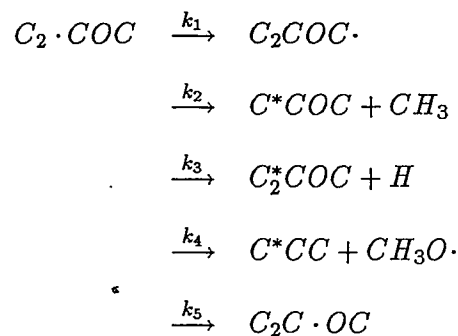


Figure 4.28 Predicted Rate Constants for C<sub>2</sub>OOC. Dissociation as a Function of Temperature at 1 atm with N<sub>2</sub> as Bath Gas



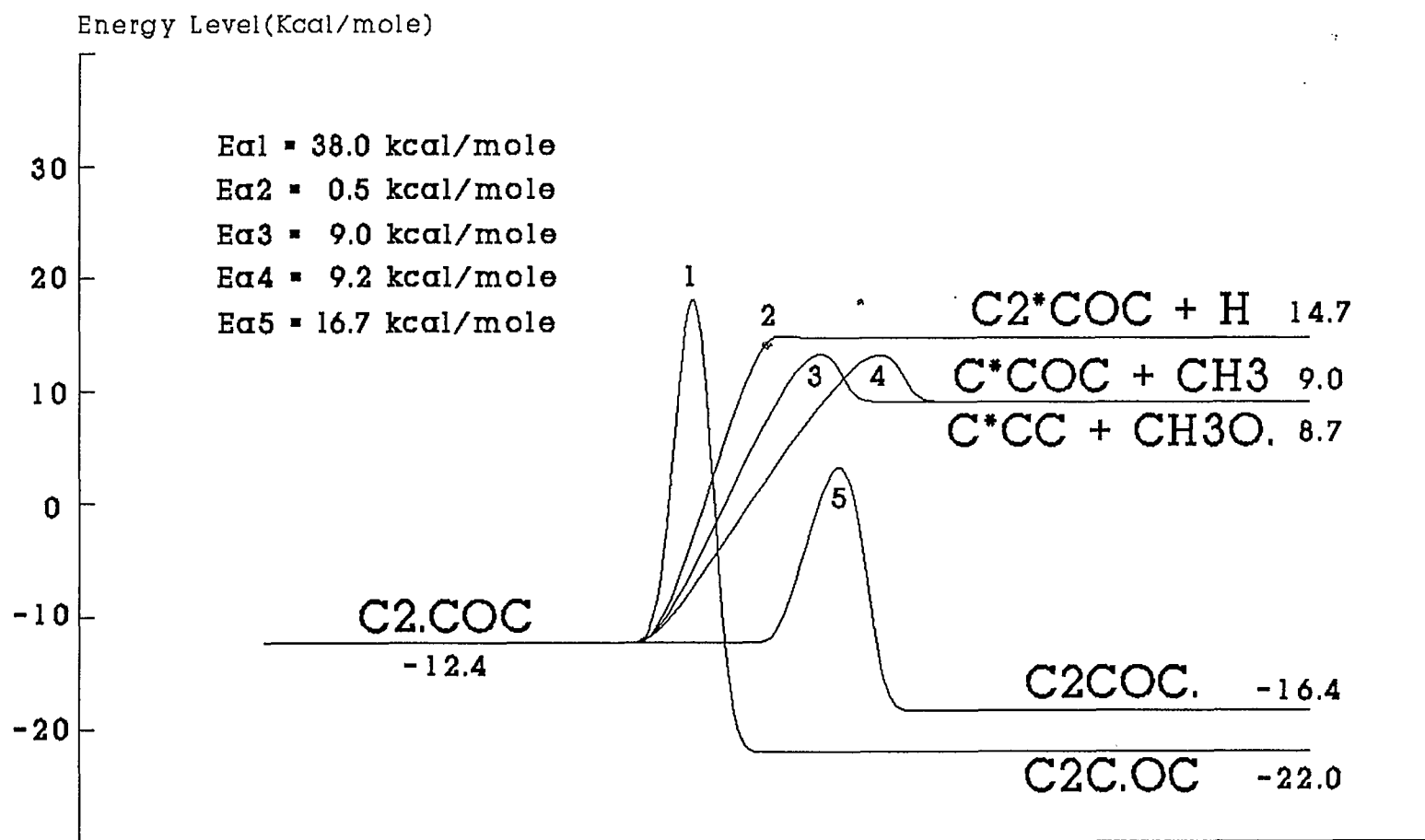
### 4.2.9 Unimolecular Dissociation of $C_2 \cdot COC$

The energy diagram and calculation results, are shown in Fig 4.29, 4.30 and 4.31 for the  $C_2 \cdot COC$  unimolecular dissociation reaction system.

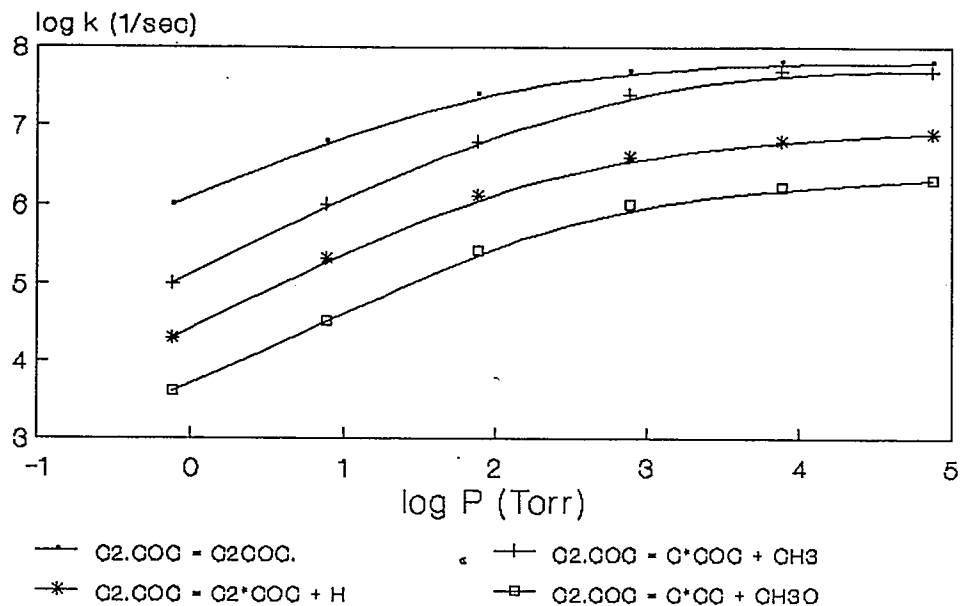


The rate constants of these reactions are below their high pressure limit at atmospheric pressure and 1000 K. The rate constants for all channels are close to their high pressure limit when the pressure reaches 10 atm. Reaction (1) and (2) are dominant.

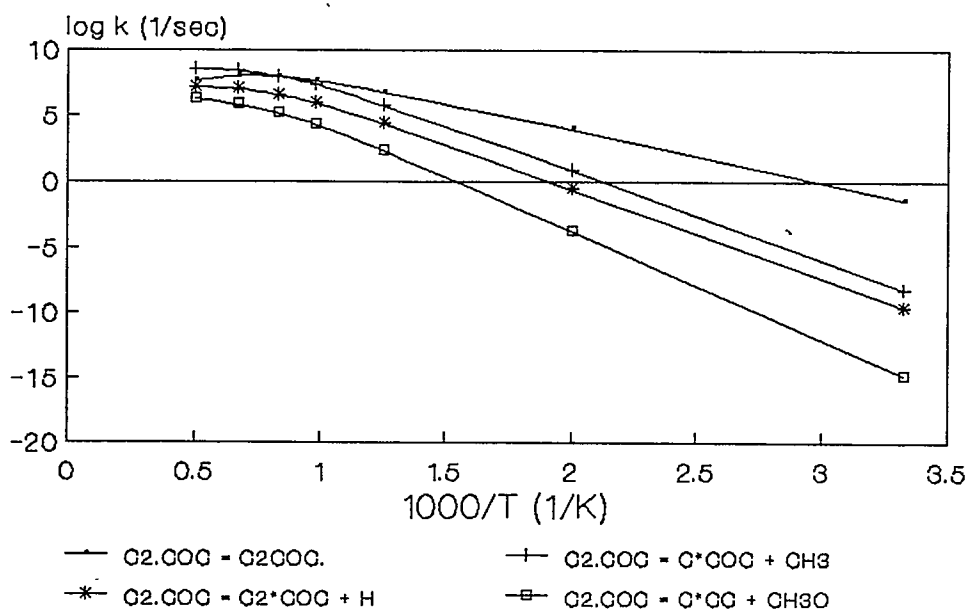
Detailed output results for  $C_2 \cdot COC$  unimolecular reaction are presented in Appendix B.9 which list the kinetic parameters for the temperature and pressure ranges of 800 to 1200 K and 7.6 to 760 Torr.

Figure 4.29 Energy Diagram of C<sub>2</sub>.COC

**Figure 4.30 Predicted Rate Constants for C<sub>2</sub>COG Dissociation as a Function of Pressure at 1024 K with N<sub>2</sub> as Bath Gas**



**Figure 4.31 Predicted Rate Constants for C<sub>2</sub>COG Dissociation as a Function of Temperature at 1 atm with N<sub>2</sub> as Bath Gas**



### 4.3 Kinetic Mechanism and Modeling

A detailed reaction kinetic mechanism was developed to describe the MTBE oxidation reaction system. of reactions studied. Elementary reaction rate parameters for abstraction reactions are based upon evaluated literature comparison, thermodynamics, Transition State Theory determination of Arrhenius A factor and energies of activation when literature data was not available. QRRK calculation<sup><21,22></sup>, as described in previous section, were used to estimate apparent rate parameters for dissociation reactions (specially at 1 atm) reported for a temperature range of 800 to 1200 K and at pressure of 7.6 to 760 Torr for  $N_2$  as bath gas.

Model predictions and experimental data of Norton *et al*<sup><14></sup>. are shown in Fig 4.32 which show only a small difference between calculated and experimental values for reactants and main products. The kinetic parameters estimated for several of the elementary reactions in detailed mechanism, are estimated based on best available thermodynamic and kinetic data in literature or for similar reactions.

In order to find out the most influential reactions in the detailed mechanism, a sensitivity analysis (computer code SENS) was applied and results are shown in Fig 4.33 and 4.34.

Figure 4.32 Model of Product Distribution vs. Time

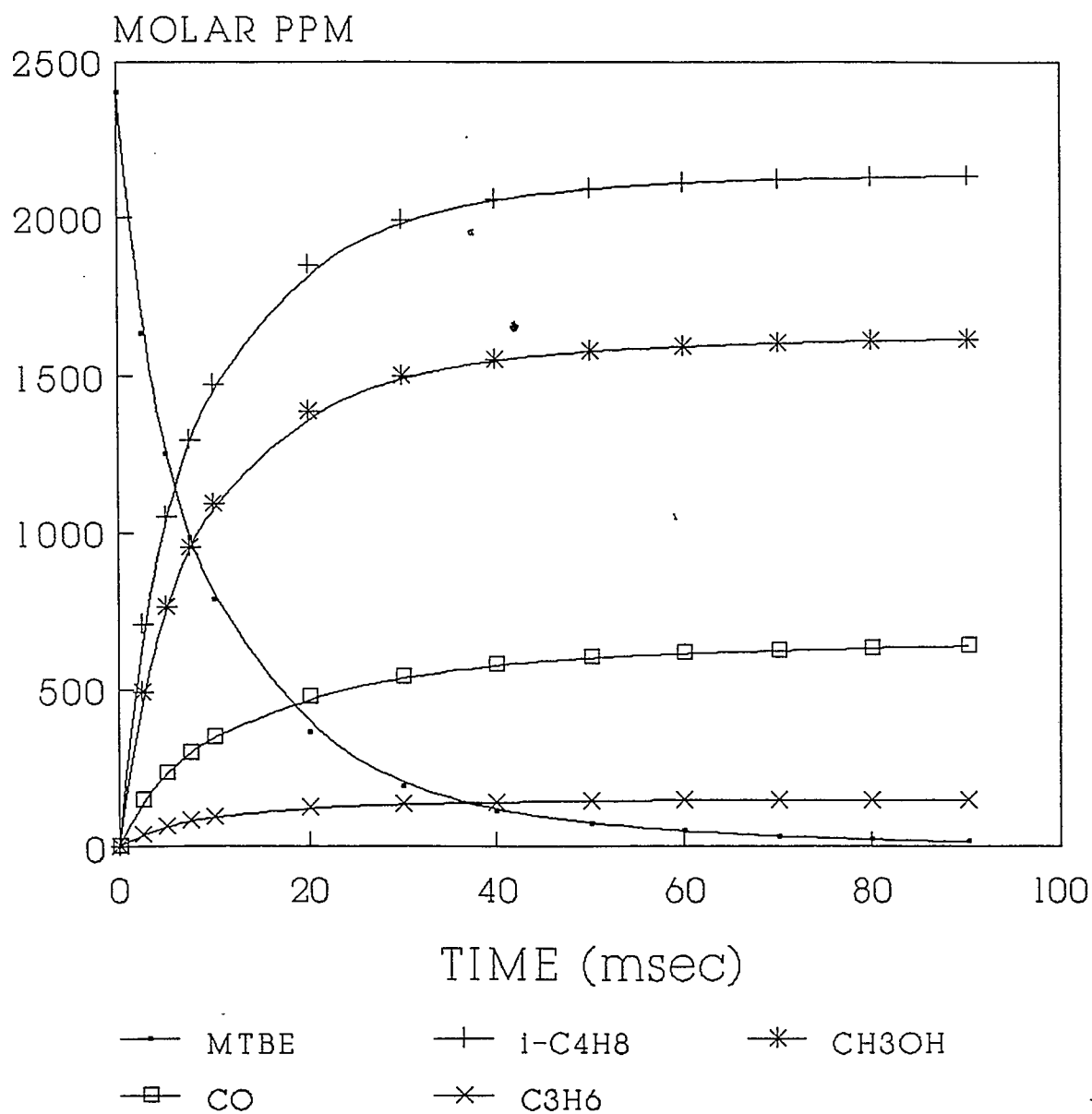
**T=1024K, PHI=0.96**

Figure 4.33 Experimental Product Distribution vs. Time (by Norton et.al.)

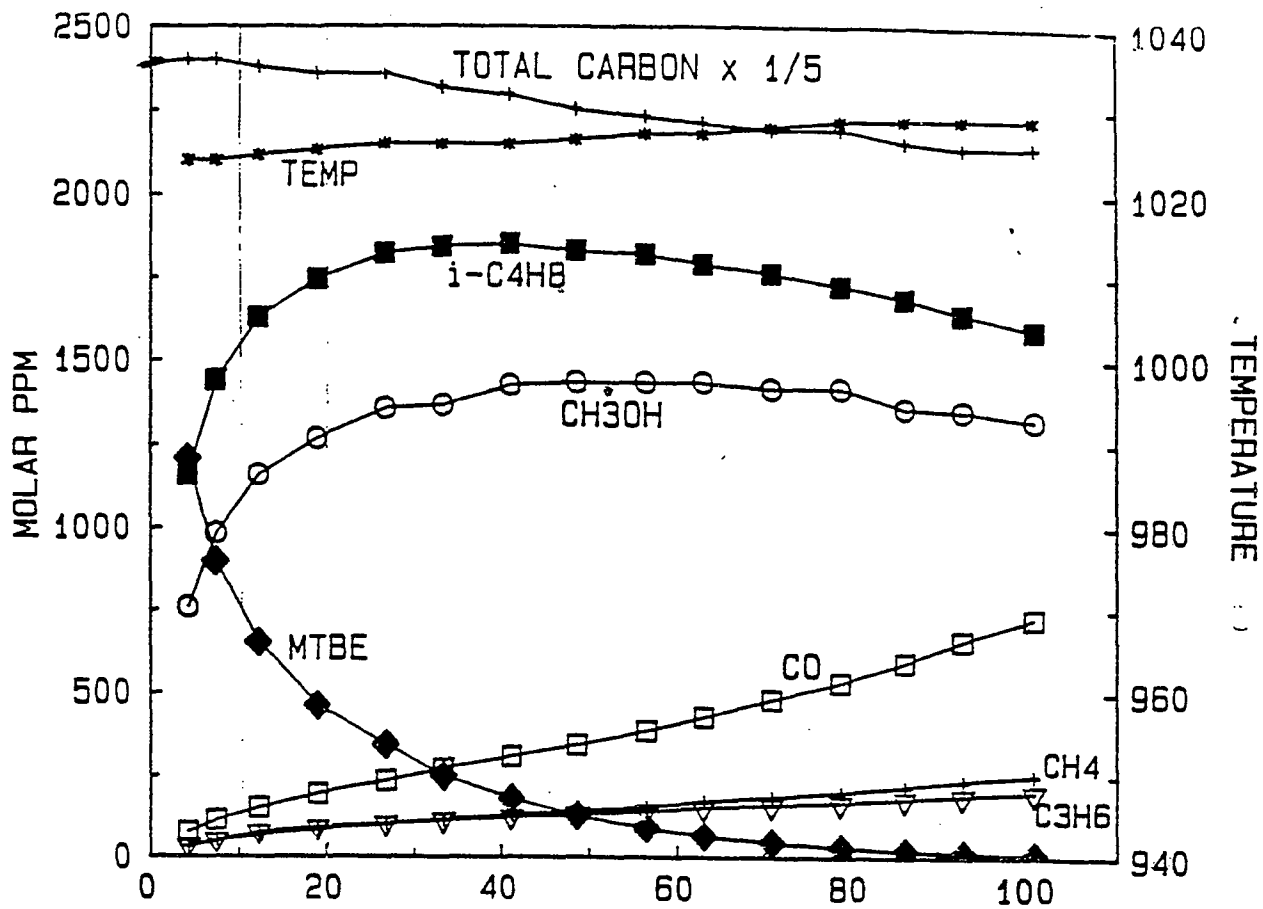


Table 4.1: Detailed Mechanism for  $C_3COC$  oxidation System

P = 1 atm. Temperature range : 800 ~ 1200K

No.	REACTION	A	n	$E_a$	source
1.	$H_2 + N_2 = H + H + N_2$	4.58E+19	-1.40	104377.	1
2.	$O_2 + N_2 = O + O + N_2$	9.81E+24	-2.50	116001.	1
3.	$O_2 + H_2 = H + HO_2$	1.44E+14	0.0	56630.	1
4.	$H + O_2 = OH + O$	3.38E+17	-0.90	17386.	1
5.	$O + H_2 = OH + H$	1.08E+04	2.80	5921.	1
6.	$OH + N_2 = O + H + N_2$	2.41E+15	0.0	99350.	1
7.	$OH + H_2 = H + H_2O$	6.38E+06	2.00	2961.	1
8.	$OH + O_2 = O + HO_2$	2.23E+14	0.0	52656.	1
9.	$OH + OH = H_2O + O$	2.11E+08	1.40	397.	1
10.	$HO_2 + N_2 = H + O_2 + N_2$	1.20E+19	-1.18	48409.	1
11.	$HO_2 + H_2 = H_2O_2 + H$	3.01E+14	0.0	26230.	1
12.	$HO_2 + H = 2OH$	1.69E+14	0.0	874.	1
13.	$HO_2 + OH = H_2O + O_2$	1.44E+16	-1.0	0.	1
14.	$HO_2 + HO_2 = H_2O_2 + O_2$	1.81E+12	0.0	0.	1
15.	$H_2O_2 + N_2 = OH + OH + N_2$	1.29E+33	-4.86	53242.	1
16.	$H_2O_2 + H = H_2O + OH$	2.41E+13	0.0	3974.	1
17.	$H_2O_2 + O = OH + HO_2$	9.63E+06	2.0	3974.	1
18.	$H_2O_2 + OH = H_2O + HO_2$	5.76E+11	0.0	318.	1
19.	$H_2O + N_2 = H + OH + N_2$	3.49E+15	0.0	105112.	1
20.	$HCO + O_2 = CO + HO_2$	2.56E+14	0.0	1690.	1

No.	REACTION	A	n	$E_a$	source
21.	$\text{HCO} + \text{H} = \text{H}_2 + \text{CO}$	1.20E+14	0.0	0.	1
22.	$\text{HCO} + \text{O} = \text{H} + \text{CO}_2$	3.01E+13	0.0	0.	1
23.	$\text{HCO} + \text{O} = \text{OH} + \text{CO}$	3.01E+13	0.0	0.	1
24.	$\text{HCO} + \text{OH} = \text{H}_2\text{O} + \text{CO}$	3.01E+13	0.0	0.	1
25.	$\text{HCO} + \text{HO}_2 = \text{OH} + \text{H} + \text{CO}_2$	3.01E+13	0.0	0.	1
26.	$\text{CO} + \text{OH} = \text{CO}_2 + \text{H}$	1.71E+11	0.0	0.	1
27.	$\text{CO} + \text{HO}_2 = \text{CO}_2 + \text{OH}$	1.50E+14	0.0	23700.	1
28.	$\text{CO} + \text{O} + \text{N}_2 = \text{CO}_2 + \text{N}_2$	6.16E+14	0.0	3000.	1
29.	$\text{CO} + \text{O}_2 = \text{CO}_2 + \text{O}$	2.53E+12	0.0	47688.	1
30.	$\text{HCO} + \text{N}_2 = \text{H} + \text{CO} + \text{N}_2$	5.12E+21	-2.14	20422.	1
31.	$\text{CH}_4 = \text{CH}_3 + \text{H}$	2.77E+30	-4.654	109726.	2
32.	$\text{CH}_4 + \text{H} = \text{CH}_3 + \text{H}_2$	2.20E+04	3.00	8750.	2
33.	$\text{CH}_4 + \text{O} = \text{CH}_3 + \text{OH}$	1.02E+09	1.50	8600.	2
34.	$\text{CH}_4 + \text{O}_2 = \text{CH}_3 + \text{HO}_2$	4.00E+13	0.0	56900.	2
35.	$\text{CH}_4 + \text{OH} = \text{CH}_3 + \text{H}_2\text{O}$	1.90E+05	2.40	2110.	2
36.	$\text{CH}_4 + \text{HO}_2 = \text{CH}_3 + \text{H}_2\text{O}_2$	1.80E+11	0.0	18600.	2
37.	$\text{CH}_3 + \text{CH}_3 = \text{C}_2\text{H}_4 + \text{H}_2$	5.00E+15	0.0	32000.	2
38.	$\text{CH}_3 + \text{CH}_3 = \text{C}_2\text{H}_5 + \text{H}$	1.80E+12	0.0	10400.	2
39.	$\text{CH}_3 + \text{O}_2 = \text{CH}_3\text{O} + \text{O}$	5.39E+15	-0.714	31188.	2
40.	$\text{CH}_3 + \text{O}_2 = \text{CH}_2\text{O} + \text{OH}$	1.22E+14	-0.712	17588.	2

No.	REACTION	A	n	$E_a$	source
41.	$\text{CH}_3 + \text{OH} = \text{C}_2\text{H}_2\text{OH} + \text{H}$	1.24E+19	-1.679	8784.	2
42.	$\text{CH}_3 + \text{OH} = \text{CH}_2 + \text{H}_2\text{O}$	4.19E+18	-1.679	8784.	2
43.	$\text{CH}_3 + \text{HO}_2 = \text{CH}_3\text{OOH}$	4.67E+30	-5.926	3972.	2
44.	$\text{CH}_3 + \text{HO}_2 = \text{CH}_3\text{O} + \text{OH}$	2.24E+14	-0.248	693.	2
45.	$\text{CH}_3 + \text{CH}_3\text{OO} = \text{CH}_3\text{O} + \text{CH}_3\text{O}$	1.00E+13	0.0	0.	2
46.	$\text{CH}_2 + \text{O}_2 = \text{HCO} + \text{OH}$	8.60E+10	0.0	-500.	2
47.	$\text{CH}_2 + \text{O}_2 = \text{CO}_2 + \text{H}_2$	6.90E+11	0.0	500.	2
48.	$\text{CH}_2 + \text{O}_2 = \text{CO}_2 + \text{H} + \text{H}$	1.60E+12	0.0	1000.	2
49.	$\text{CH}_2 + \text{O}_2 = \text{CO} + \text{H}_2\text{O}$	1.90E+10	0.0	-1000.	2
50.	$\text{CH}_2 + \text{O}_2 = \text{CO} + \text{H} + \text{OH}$	8.60E+10	0.0	-500.	2
51.	$\text{CH}_2 + \text{O}_2 = \text{CH}_2\text{O} + \text{O}$	5.00E+13	0.0	9000.	2
52.	$\text{CH}_3\text{O} + \text{H} = \text{CH}_2\text{O} + \text{H}_2$	1.99E+13	0.0	0.	2
53.	$\text{CH}_3\text{O} + \text{OH} = \text{CH}_2\text{O} + \text{H}_2\text{O}$	1.81E+13	0.0	0.	2
54.	$\text{CH}_3\text{O} + \text{HO}_2 = \text{CH}_2\text{O} + \text{H}_2\text{O}_2$	3.01E+11	0.0	0.	2
55.	$\text{CH}_3\text{O} + \text{HCO} = \text{CH}_3\text{OH} + \text{CO}$	9.04E+13	0.0	0.	2
56.	$\text{CH}_3\text{O} + \text{CO} = \text{CH}_3 + \text{CO}_2$	1.57E+13	0.0	11761.	2
57.	$\text{CH}_3\text{O} + \text{CH}_2\text{O} = \text{CH}_3\text{OH} + \text{HCO}$	1.02E+11	0.0	2970.	2
58.	$\text{CH}_3\text{O} + \text{CH}_4 = \text{CH}_3\text{OH} + \text{CH}_3$	1.57E+11	0.0	8811.	2
59.	$\text{CH}_3\text{O} + \text{C}_2\text{H}_4 = \text{CH}_3\text{OH} + \text{C}_2\text{H}_3$	1.21E+11	0.0	6732.	2
60.	$\text{CH}_3\text{O} + \text{C}_2\text{H}_6 = \text{CH}_3\text{OH} + \text{C}_2\text{H}_5$	2.40E+11	0.0	7069.	2

No.	REACTION	A	n	$E_a$	source
61.	$\text{CH}_2\text{O} = \text{HCO} + \text{H}$	2.39E+20	0.0	96548.	1
62.	$\text{CH}_2\text{O} + \text{H} = \text{HCO} + \text{H}_2$	2.00E+13	0.0	3670.	2
63.	$\text{CH}_2\text{O} + \text{O} = \text{HCO} + \text{OH}$	1.80E+13	0.0	3080.	2
64.	$\text{CH}_2\text{O} + \text{OH} = \text{HCO} + \text{H}_2\text{O}$	3.40E+09	1.180	447.	2
65.	$\text{CH}_2\text{O} + \text{HO}_2 = \text{HCO} + \text{H}_2\text{O}_2$	2.00E+12	0.0	11700.	2
66.	$\text{CH}_2\text{O} + \text{O}_2 = \text{HCO} + \text{HO}_2$	2.00E+13	0.0	38900.	4
67.	$\text{CH}_2\text{O} + \text{CH}_3 = \text{HCO} + \text{CH}_4$	2.10E+03	2.810	5860.	2
68.	$\text{CH}_2\text{O} + \text{C}_2\text{H}_5 = \text{HCO} + \text{C}_2\text{H}_6$	6.00E-02	4.00	4600.	4
69.	$\text{CH}_3\text{OH} = \text{CH}_3 + \text{OH}$	1.90E+16	0.0	91784.	4
70.	$\text{CH}_3\text{OH} = \text{C.H}_2\text{OH} + \text{H}$	2.00E+17	0.0	75500.	37
71.	$\text{C}_2\text{C}^*\text{C} = \text{CH}_3 + \text{C}^*\text{CC}$	1.82E+18	0.0	90000.	38
72.	$\text{CH}_3\text{OH} + \text{O}_2 = \text{C.H}_2\text{OH} + \text{HO}_2$	2.05E+13	0.0	45000.	4
73.	$\text{CH}_3\text{OH} + \text{C.H}_2\text{OH} = \text{CH}_3\text{O.} + \text{CH}_3\text{OH}$	7.89E+09	0.0	12061.	4
74.	$\text{CH}_3\text{OH} + \text{C}_2\text{H}_3 = \text{C.H}_2\text{OH} + \text{C}_2\text{H}_4$	2.64E+09	3.20	3609.	4
75.	$\text{CH}_3\text{OH} + \text{C}_2\text{H}_5 = \text{C}_2\text{H}_6 + \text{C.H}_2\text{OH}$	6.75E+08	3.10	9160.	4
76.	$\text{CH}_3\text{OH} + \text{H} = \text{CH}_3\text{O.} + \text{H}_2$	2.60E+03	3.00	8250.	2
77.	$\text{CH}_3\text{OH} + \text{H} = \text{C.H}_2\text{OH} + \text{H}_2$	6.30E+06	2.10	4870.	2
78.	$\text{CH}_3\text{OH} + \text{OH} = \text{H}_2\text{O} + \text{CH}_3\text{O.}$	2.60E+05	2.00	2500.	2
79.	$\text{CH}_3\text{OH} + \text{OH} = \text{H}_2\text{O} + \text{C.H}_2\text{OH}$	1.90E+06	2.00	-2110.	1
80.	$\text{CH}_3\text{OH} + \text{HO}_2 = \text{H}_2\text{O}_2 + \text{C.H}_2\text{OH}$	1.70E+11	0.0	13000.	3

No.	REACTION	A	n	$E_a$	source
81.	$\text{CH}_3\text{OH} + \text{O} = \text{OH} + \text{CH}_3\text{O}.$	1.00E+13	0.0	4683.	3
82.	$\text{CH}_3\text{OH} + \text{O} = \text{OH} + \text{C.H}_2\text{OH}$	1.72E+13	0.0	4914.	3
83.	$\text{C.H}_2\text{OH} = \text{CH}_2\text{O} + \text{H}$	7.00E+14	0.0	29634.	4
84.	$\text{C.H}_2\text{OH} + \text{H} = \text{CH}_2\text{O} + \text{H}_2$	6.03E+12	0.0	0.	4
85.	$\text{C.H}_2\text{OH} + \text{CH}_2\text{O} = \text{HCO} + \text{CH}_3\text{OH}$	4.65E+10	2.80	5682.	4
86.	$\text{C.H}_2\text{OH} + \text{C}_2\text{H}_5 = \text{CH}_3\text{OH} + \text{C}_2\text{H}_4$	2.41E+12	0.0	0.	4
87.	$\text{C}_3\text{COC} = \text{C}_3\text{C} + \text{CH}_3\text{O}.$	9.84E+17	0.0	77300.	5
88.	$\text{C}_3\text{COC} = \text{C}_3\text{CO} + \text{CH}_3$	3.96E+16	0.0	83000.	5
89.	$\text{C}_3\text{COC} = \text{C}_2\text{C.OC} + \text{CH}_3$	2.26E+17	0.0	83700.	5
90.	$\text{C}_3\text{COC} = \text{C}_3.\text{COC} + \text{H}$	1.72E+16	0.0	99700.	5
91.	$\text{C}_3\text{COC} = \text{C}_3\text{COC} + \text{H}$	6.13E+14	0.0	93400.	5
92.	$\text{C}_3\text{COC} + \text{O} = \text{C}_3.\text{COC} + \text{OH}$	1.90E+05	2.68	3720.	13
93.	$\text{C}_3\text{COC} + \text{O} = \text{C}_3\text{COC} + \text{OH}$	1.86E+13	0.0	3306.	14
94.	$\text{C}_3\text{COC} + \text{H} = \text{C}_3.\text{COC} + \text{H}_2$	1.95E+06	0.0	6760.	15
95.	$\text{C}_3\text{COC} + \text{H} = \text{C}_3\text{COC} + \text{H}_2$	8.00E+12	0.0	5951.	16
96.	$\text{C}_3\text{COC} + \text{O}_2 = \text{C}_3.\text{COC} + \text{HO}_2$	6.06E+13	0.0	50867.	17
97.	$\text{C}_3\text{COC} + \text{O}_2 = \text{C}_3\text{COC} + \text{HO}_2$	1.00E+13	0.0	44900.	17
98.	$\text{C}_3\text{COC} + \text{OH} = \text{C}_3.\text{COC} + \text{H}_2\text{O}$	1.00E+07	2.00	840.	18
99.	$\text{C}_3\text{COC} + \text{OH} = \text{C}_3\text{COC} + \text{H}_2\text{O}$	7.76E+12	0.0	769.	18
100.	$\text{C}_3\text{COC} + \text{HO}_2 = \text{C}_3.\text{COC} + \text{H}_2\text{O}_2$	2.52E+11	0.0	12000.	19

No.	REACTION	A	n	$E_a$	source
101.	$C_3COC + HO_2 = C_3COC. + H_2O_2$	8.50E+10	0.0	13000.	19
102.	$C_3COC + CH_3 = C_3.COC + CH_4$	1.19E+11	0.0	11600.	20
103.	$C_3COC + CH_3 = C_3COC. + CH_4$	2.46E+12	0.0	12073.	21
104.	$C_3COC + CH_3O. = C_3.COC + CH_3OH$	3.62E+11	0.0	7094.	22
105.	$C_3COC + CH_3O. = C_3COC. + CH_3OH$	1.20E+11	0.0	3500.	22
106.	$C_3COC + C_2H_5 = C_3.COC + C_2H_6$	4.74E+11	0.0	12300.	20
107.	$C_3COC + C_2H_5 = C_3COC. + C_2H_6$	1.58E+11	0.0	12300.	20
108.	$C_3COC + C_3C. = C_3.COC + C_3C$	1.50E+11	0.0	12900.	20
109.	$C_3COC + C_3C. = C_3COC. + C_3C$	5.01E+10	0.0	12900.	20
110.	$C_3COC + CC.C = C_3.COC + CCC$	1.50E+11	0.0	12900.	20
111.	$C_3COC + CC.C = C_3COC. + CCC$	5.01E+10	0.0	12900.	20
112.	$C_3COC. = C_3C. + CH_2O$	3.02E+10	0.0	7830.	9
113.	$C_3COC. = C_3.COC$	2.84E+08	0.0	10800.	9
114.	$C_3.COC = C_2C^*C + CH_3O.$	1.09E+12	0.0	17900.	8
115.	$C_3.COC = C_2^*COC + CH_3$	8.66E+10	0.0	19000.	8
116.	$C_2COC. = C_2C.OC$	7.17E+07	0.0	1990.	11
117.	$C_2COC. = C_2.COC$	1.64E+07	0.0	6720.	11
118.	$C_2C.OC = C_2C^*O + CH_3$	8.18E+08	0.0	-869.	10
119.	$C_2C.OC = C_2^*COC + H$	1.32E+09	0.0	32100.	10
120.	$C_2.COC = C^*CC + CH_3O.$	1.42E+11	0.0	24500.	12

No.	REACTION	A	n	$E_a$	source
121.	$C2.COC = C2^*COC + H$	1.91E+11	0.0	22300.	12
122.	$C2.COC = C2C.OC$	6.44E+10	0.0	30700.	12
123.	$C3C. = C2CC.$	1.37E+13	0.0	40700.	6
124.	$C3C. = C2C^*C + H$	6.00E+12	0.0	33800.	6
125.	$C3C. + H = C2C^*C + H2$	5.43E+12	0.0	0.	23
126.	$C2CC. + H = C2C^*C + H2$	1.81E+12	0.0	0.	23
127.	$C3C. + OH = C2C^*C + H2O$	7.23E+13	0.0	0.	24
128.	$C2CC. + OH = C2C^*C + H2O$	2.41E+13	0.0	0.	24
129.	$C3C. + HO2 = C2C^*C + H2O2$	9.03E+11	0.0	0.	25
130.	$C2CC. + HO2 = C2C^*C + H2O2$	3.01E+11	0.0	0.	25
131.	$C3C. + CH3 = C2C^*C + CH4$	3.39E+12	0.50	0.	26
132.	$C2CC. + CH3 = C2C^*C + CH4$	1.13E+12	0.50	0.	26
133.	$C3C. + CH3O. = C2C^*C + CH3OH$	7.20E+12	0.50	0.	27
134.	$C2CC. + CH3O. = C2C^*C + CH3OH$	2.40E+12	0.50	0.	28
135.	$C3C. + C.H2OH = C2C^*C + CH3OH$	7.21E+11	0.0	0.	29
136.	$C2CC. + C.H2OH = C2C^*C + CH3OH$	2.40E+11	0.0	0.	30
137.	$C3C. + CH2O = C3C + HCO$	6.00E-02	4.00	4600.	31
138.	$C2CC. + CH2O = C3C + HCO$	3.00E-02	4.00	5600.	32
139.	$C3C. + CH3OH = C.H2OH + C3C$	1.70E-02	4.00	7000.	2
140.	$C3C. + CH3OH = CH3O. + C3C$	7.50E-03	4.00	11000.	2

No.	REACTION	A	n	$E_a$	source
141.	$C_2CC. + CH_3OH = C.H_2OH + C_3C$	3.30E-02	4.00	6000.	2
142.	$C_2CC. + CH_3OH = CH_3O. + C_3C$	1.30E-02	4.00	10000.	2
143.	$C_3C. + O_2 = C_2C^*C + HO_2$	1.77E+09	0.0	-4520.	35
144.	$C_3C + O_2 = HO_2 + C_3C.$	2.00E+13	0.0	43000.	35
145.	$C_3C + O_2 = HO_2 + C_2CC.$	4.00E+13	0.0	50900.	35
146.	$C_2CC. = C^*CC + CH_3$	6.51E+12	0.0	29100.	7
147.	$C_2CC. = C_2C^*C + H$	9.97E+11	0.0	29000.	7
148.	$C_2C^*C + CH_3O. = C_2.C^*C + CH_3OH$	2.00E+12	0.0	8000.	36
149.	$C_2C^*C + C.H_2OH = C_2.C^*C + CH_3OH$	2.00E+11	0.0	9000.	36
150.	$C^*CC + CH_3O. = C^*CC. + CH_3OH$	1.00E+12	0.0	8000.	36
151.	$C^*CC + C.H_2OH = C^*CC. + CH_3OH$	1.00E+11	0.0	9000.	36
152.	$C_2H_2 + CH_3 = CC^*C.$	5.22E+32	-6.256	17525.	2
153.	$C_2H_2 + CH_3 = C\#CC + H$	5.81E+15	-1.126	21284.	2
154.	$C_2H_2 + CH_3 = C^*C^*C + H$	7.32E+27	-4.395	38603.	2
155.	$C_2H_3 = C_2H_2 + H$	4.52E+26	-4.266	50497.	2
156.	$C_2H_3 + CH_3 = C_2H_2 + CH_4$	3.90E+11	0.0	0.	2
157.	$C_2H_4 + H = C_2H_3 + H_2$	1.30E+06	2.53	12200.	2
158.	$C_2H_4 + CH_3 = C_2H_3 + CH_4$	4.20E+11	0.0	11100.	2
159.	$C_2H_4 + CH_3 = C^*CC + H$	4.37E+20	-2.399	26602.	2
160.	$C_2H_5 + CH_3 = C_2H_4 + CH_4$	3.60E+11	0.0	-1030.	2

No.	REACTION	A	n	$E_a$	source
161.	$C_2H_5 + C_2H_3 = C_2H_4 + C_2H_4$	4.80E+11	0.0	0.	2
162.	$C_2H_5 + C_2H_3 = C_2H_6 + C_2H_2$	4.80E+11	0.0	0.	2
163.	$C_2H_5 + C_2H_4 = C_2H_6 + C_2H_3$	6.30E+02	3.13	18000.	2
164.	$C_2H_6 + H = C_2H_5 + H_2$	5.40E+02	3.50	5200.	2
165.	$C_2H_6 + CH_3 = C_2H_5 + CH_4$	2.70E-01	4.00	8285.	2
166.	$C\#CC + H = C\#CC. + H_2$	5.00E+13	0.0	5000.	2
167.	$C\#CC + H = C^*C^*C + H^*$	1.04E+20	-1.821	17854.	2
168.	$C\#CC + H = CC^*C.$	2.59E+34	-6.587	12401.	2
169.	$C\#CC + H = C^*CC.$	3.23E+28	-4.487	16297.	2
170.	$C\#CC + CH_3 = C\#CC. + CH_4$	3.80E+11	0.0	9000.	2
171.	$C^*C^*C + H = C^*CC.$	5.66E+22	-3.026	7536.	2
172.	$C^*C^*C + H = CC^*C.$	6.38E+25	-4.047	14693.	2
173.	$C^*C^*C + H = C\#CC. + H_2$	5.00E+13	0.0	5000.	2
174.	$C^*C^*C + CH_3 = C_2.C^*C$	6.60E+10	0.0	7990.	2
175.	$C^*C^*C + CH_3 = C\#CC. + CH_4$	3.80E+11	0.0	9000.	2
176.	$C^*CC. + H = C^*C^*C + H_2$	3.60E+12	0.0	0.	2
177.	$C^*CC. + CH_3 = C^*C^*C + CH_4$	8.92E+11	0.0	-1571.	2
178.	$C^*CC. + CH_3O. = C^*C^*C + CH_3OH$	1.00E+13	0.0	0.	2
179.	$C^*CC. + C_2H_5 = C^*C^*C + C_2H_6$	2.40E+12	0.0	0.	2
180.	$C^*CC. + C_2H_5 = C^*CC + C_2H_4$	1.20E+12	0.0	0.	2

No.	REACTION	A	n	$E_a$	source
181.	$C^*CC. + C^*CC. = C^*CC + C^*C^*C$	1.00E+12	0.0	0.	2
182.	$C^*CC + H = C^*CC. + H_2$	5.00E+13	0.0	5000.	2
183.	$C^*CC + CH_3 = C^*CC. + CH_4$	3.80E+11	0.0	9000.	2
184.	$C^*CC + C_2H_5 = C^*CC. + C_2H_6$	3.80E+11	0.0	9000.	2
185.	$CCC. = C^*CC + H$	1.20E+13	0.0	38500.	2
186.	$CCC. = C_2H_4 + CH_3$	1.00E+13	0.0	32900.	2
187.	$CCC. + CH_3O. = C^*CC + CH_3OH$	5.00E+12	0.0	0.	2
188.	$CCC + H = CC.C + H_2$	1.30E+06	2.40	4470.	2
189.	$CCC + H = CCC. + H_2$	1.30E+06	2.54	6760.	2
190.	$CCC + CH_3 = CC.C + CH_4$	9.00E-02	4.00	6285.	2
191.	$CCC + CH_3 = CCC. + CH_4$	2.70E-01	4.00	8285.	2
192.	$CC.C + CH_3 = C_3C$	1.03E+15	-0.645	-83.	2
193.	$C_2.C^*C + C^*CC. = C_2C^*C + C^*C^*C$	2.40E+12	0.0	0.	2
194.	$C_2C^*C = C_2.C^*C + H$	3.98E+15	0.0	80160.	2
195.	$C_2C^*C + H = C_2.C^*C + H_2$	1.30E+14	0.0	5000.	2
196.	$C_2CC. = C_2C^*C + H$	6.00E+12	0.0	33800.	2

# High pressure limit value

\* Pressure dependent : rate expression given for 760 torr

Temperature range : 973 - 1073 ° K

DISSOC : apparent rate constant by *DISSOCIATION* computer code calculation.

(QRRK) other parameter input to DISSOC calculation.

QRRK : apparent rate constant by *CHEMACT* computer code calculation

#### Sources of Rate Constants

1. Tsang, W.; Hampson, R. F. *J. Phys. Chem. Ref. Data* 1986, 15, 3, 1087.
2. Dean, A. M. *J. Phys. Chem.* 1989, 93.
3. Fitted data from NIST database.
4. Tsang, W. *J. Phys. Chem. Ref. Data* 1987, 16, 471.
5. DISSOC 1 in Appendix B.1.
6. DISSOC 2 in Appendix B.2.
7. DISSOC 3 in Appendix B.3.
8. DISSOC 4 in Appendix B.4.
9. DISSOC 5 in Appendix B.5.
10. DISSOC 6 in Appendix B.6.

11. DISSOC 7 in Appendix B.7.
12. DISSOC 8 in Appendix B.8.
13. Kerr, J. A.; Moss, S. J. *Handbook of Bimolecular and Termolecular Gas Reaction*, Vol. I & II, CRC Press Inc., 1981.
14. Taken fitted data of ( $CO + O \rightarrow$ ) from NIST database.
15. Allara, D. L.; Show, R. J. *J. Phys. Chem. Ref. Data* 1980, 9, 523.
16. Taken as fitted data of ( $CO + H \rightarrow$ ) from NIST database.
17. Taken as ( $CH_3OH + O_2 \rightarrow$ ) and  $2/3 \times (C_2H_6 + O_2 \rightarrow)$ .
18. Optimization of OH abstraction to HCs'.
19. *23th Int'l Symposium on Combustion* 1990, 888.
20. Taken as the corresponding HCs' from Allra and Show.
21.  $1/2 \times (CO + CH_3 \rightarrow)$ .
22.  $3/2 \times (CH_3O. + C_2H_6 \rightarrow)$ .
23.  $3 \times (CC. + H \rightarrow)$  and ( $CC. + H \rightarrow$ ).
24.  $3 \times (CC. + OH \rightarrow)$  and ( $CC. + OH \rightarrow$ ).
25.  $3 \times (CC. + HO_2 \rightarrow)$  and ( $CC. + HO_2 \rightarrow$ ).
26.  $3 \times (CC. + CH_3 \rightarrow)$  and ( $CC. + CH_3 \rightarrow$ ).

27. Taken as  $(C_3C + CC \rightarrow)$ .
28. Taken as  $(C_3C + CC \rightarrow)$ .
29.  $3 \times (CH_2OH + C_2H_5 \rightarrow)$ .
30. Taken as  $(CH_2OH + C_2H_5 \rightarrow)$ .
31. Taken as  $(CH_2O + C_2H_5 \rightarrow)$ .
32.  $1/2 \times (CH_2O + C_2H_5 \rightarrow)$ .
33. Yu, Hui, M. Sc., Thesis, NJIT(1990).
34. Estimated from  $(C_2H_4 + CH_3O \rightarrow)$  and  $(C_2H_4 + CH_2OH \rightarrow)$ .
35. Hidaka, Y.; Oki, T.; Kawano, H. *J. Phys. Chem.* **1989**, *93*, 7134.
36. Bradley, J. N.; West, K. O. *J. Chem. Soc. Faraday Trans.* **1976**, *72*, 558.

Figure 4.33 Sensitivity Analysis Summary  
Temp. = 1024K, R.T. = 0.1 sec.

Species	Reaction Number	
	Most Important $10^{-2} \leq  S  \leq 1$	Important $10^{-3} \leq  S  \leq 10^{-2}$
$C_3CO$	+ 3,7,8,13,14,27,30,32,34,62,64	11,61,75,76,178
	+ 69,113,114,125,132,195,196	
	- 4,10,12,15,20,44,65,70,77,80,81	27,35,40,83,130,182,195,196
	- 87,88,94,95,96,99,115,124,144,179,194	
$C_2C^*C$	+ 87,125,144,175	4,12,77,100,115,149
	- 90,116,124,147,148	7,20,31,44,88
$CH_3OH$	+ 7,8,13,30,44,124,148,149	14,26,35,87,115,151
	- 4,10,12,15,20,88,100,101,196	32,40,61,114,125,144,195
$CO$	+ 4,12,15,19,45,80,81,82,83,84,88,147,148	10,26,40,61,87,93,94,144
	- 7,8,13,14,27,28,30,149	3,31,32,34,44,196
$CH_2O$	+ 44,123,147,148,149	35,38,62,115
	- 4,15,20,30,88	7,10,12,14,32,61,87,116,132,144,196
$CH_4$	+ 7,8,12,13,14,30,31,32,34,88,124,132	26,27,36,61,147
	- 4,10,15,35,43,44,87,125,148,196	33,62,134,144
$C^*CC$	+ 7,20,44,70,71,88,148	14,15,26,32,61,114
	- 12,77,87,144,147,196	3,4,10,13,62,64,115,116,132,134

## Chapter 5

# Conclusion

Detailed mechanisms were developed for the oxidation reactions of MTBE (methyl *tert*-butyl ether) and compared with the experimental data done by Norton et.al.

The unimolecular and bimolecular versions of Quantum RRK theory were used to develop kinetic mechanisms for the MTBE oxidations. Sensitivity analysis on these reaction mechanism was performed to identify the important reaction channels and to improve the fit of the mechanism on experimental observation.

The model results give a satisfactory fit for the conversion of MTBE with the experimental data. This mechanism indicated an acceptable path toward the formation of the major products, isobutylene and methanol. The molecular elimination is dominant when temperature lower than  $\sim 900$  K in the MTBE oxidation system. It gives

a explanation why Daly *et al.*<sup><24></sup> and Choo *et al.*<sup>< 25 ></sup> concluded that the decomposition reaction of MTBE is a four-center molecular elimination in the condition of temperature  $\sim 700$  K.

The difference between the calculation result and high pressure limit increases when the temperature is above 1000 K at atmospheric pressure. The reaction of ( $C_3COC \rightarrow CH_3O \cdot + C_3C \cdot$ ) is therefore becoming important as the temperature increasing and becoming dominant as the temperature higher than 1800 K.

A sensitivity analysis of the model<sup>†</sup> was also done to show the most important reactions in the mechanism. It is very useful to analyze this complex reaction system involving 196 elementary reactions.

## Chapter 6

### Reference

1. *Oil & Gas J.* 1988, 86, 28.
2. *Chem. & Eng. News* 1985, 63, 12.
3. Anderson, E. *Chem. & Eng. News* 1986, 64, 8.
4. *Chem. & Eng. News* 1990, 68, 9.
5. *Oil & Gas J.* 1987, 85, 24.
6. Ramirez, R. *Chem. Eng.* 1987, 94, 19.
7. *Chem. Eng.* 1986, 93, 22.
8. Al-Jarallah, A. M.; Lee, A. K. K. *Hydrocarbon Processing* 1988, 67, 51.
9. *Process Eng.* 1988, 69, 19.
10. Masters, K. R.; Prohaska, E. A. *Hydrocarbon Processing* 1988, 67, 48.

11. Lange, P. M.; Martinola, F.; Oecki, S. *Hydrocarbon Processing* 1985, 64, 51.
12. Bitar, L. S.; Hazbun, E. A.; Piel, W. J. *Hydrocarbon Processing* 1984, 63, 63.
13. Herwig, J.; Schleppinghoff, B.; Schulwitz, S. *Hydrocarbon Processing* 1984, 63, 86.
14. Norton, T. S.; Dryer, F. L. *23th Int'l Symposium on Combustion* 1990
15. Borman, S. *Chem. & Eng. News* 1989.
16. Wallington, T. J.; Dagant, P.; Liu, R.; Kurylo, M. J. *Env. Sci. Tech.* 1988, 22, 842.
17. Cox, R. A.; Goldstone, A. *Proceedings of the 2nd European Symposium on the Physico Chemical Behavior of Atmospheric Pollutants*; Riedel: Dorecht, Holland, 1988, 112.
18. Pelzer, H.; Wigner, E. *Phys. Chem.* 1932, B15, 445.
19. Glasstone, S.; Laidler, K. J.; Eyring, H. *Theory of Rate Processes*, McGraw-Hill, New York 1940.
20. Westmoreland, P. R.; Dean, A. M. *AICHE J.* 1986, 32,171.
21. Dean, A. M. *J. Phys. Chem.* 1985, 89, 4600.
22. Ritter, E.; Bozzelli; J. W.; Dean, A. M. *J. Phys. Chem.* 1988.
23. Allara, D. L.; Show, R. *J. Phys. Chem. Ref. Data* 1980, 9, 3, 523.

24. Dale, N. J.; Wentrup, C. *Aust. J. Chem.* 1968, 21, 2711.
25. Choo, K. Y.; Golden, D. M.; Benson, S. W. *Int. J. Chem. Kin.* 1974, 6, 631.
26. Brocard, J. C.; Baronnet, F. *Combust. Flame* 1983, 52, 25.
27. Dunphy, M.; Simmie, J. M. *Combust. Sci. Tech.* 1989, 66, 157.
28. *Chem. & Eng. News* 1990, 68, 17.
29. Ritter, E., PhD Thesis, NJIT(1989).

## Appendix A

# Species in Reaction Mechanism

mtbethermo

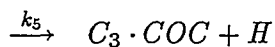
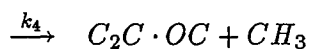
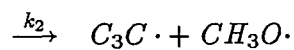
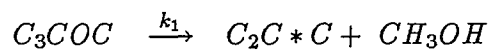
SPECIES	HF(298)	S (298)	CP300	CP500	CP800	CP1000	CP1500	CP2000
N2	0.00	45.77	6.96	7.08	7.50	7.81	8.31	8.61
C(S)	0.00	21.83	2.06	3.50	4.74	5.15	5.65	5.89
C	170.88	38.31	4.98	4.97	4.97	4.97	4.97	5.01
H2	0.00	31.21	6.90	6.99	7.10	7.21	7.72	8.17
H	52.10	27.36	4.97	4.97	4.97	4.97	4.97	4.97
CH	142.00	43.72	6.97	7.03	7.40	7.78	8.74	9.36
CH2	92.35	46.32	8.28	8.99	10.15	10.88	12.22	13.00
CH3	35.12	46.38	9.26	10.81	12.90	14.09	16.26	17.56
CH4	-17.90	44.48	8.51	11.10	15.00	17.20	20.61	22.61
C2H	132.00	49.58	8.88	10.22	11.54	12.16	13.32	14.11
C2H2	54.19	48.01	10.60	13.08	15.31	16.29	18.31	19.57
C2H3	67.10	56.20	10.89	13.87	17.16	18.73	21.34	23.20
C2H4	12.54	52.39	10.28	14.91	20.03	22.45	26.21	28.35
C2H5	28.36	57.90	12.26	17.13	22.85	25.74	30.54	33.31
C2H6	-20.24	54.85	12.58	18.68	25.80	29.33	34.91	38.37
C3H2	106.65	117.98	12.96	16.94	20.26	21.59	23.85	25.59
C3H3	77.26	89.99	14.05	18.28	22.39	24.24	27.23	28.88
C*CC.	83.30	58.51	14.06	18.27	22.42	24.25	27.21	28.85
C*C*C	45.92	58.30	14.19	19.77	25.45	28.02	32.04	34.07
C3H5	40.97	63.01	14.75	21.68	28.58	31.62	36.44	39.44
C*CC.	40.97	63.01	14.75	21.68	28.58	31.62	36.44	39.44
CC*C.	62.82	64.87	15.29	21.55	28.19	31.18	35.89	38.79
C3H6	4.88	63.80	15.26	22.67	30.66	34.43	40.48	43.87
C*CC	4.88	63.80	15.26	22.67	30.66	34.43	40.48	43.87
CCC.	23.21	68.41	16.85	25.39	34.09	38.05	44.58	48.61
CC.C	20.67	68.91	15.73	23.96	33.01	37.34	44.26	48.30
C2C.	20.67	68.91	15.73	23.96	33.01	37.34	44.26	48.30
CCC	-25.33	64.50	17.63	27.01	37.10	41.83	49.27	53.43
C3H8	-25.33	64.50	17.63	27.01	37.11	41.83	49.27	53.43
C*CC	44.32	59.30	14.56	19.71	25.06	27.72	31.85	34.00
C3H3	83.33	56.99	14.06	18.27	22.33	24.19	27.21	28.85
C2.C*C	32.10	70.80	20.84	30.45	40.03	44.36	51.21	52.50
C2C*C	-4.04	70.17	21.37	31.23	41.86	46.86	54.67	58.77
C2CC.	16.76	74.86	22.47	34.00	45.48	50.62	59.21	64.78
C3.C	16.76	74.86	22.47	34.00	45.48	50.62	59.21	64.78
CCCC	-30.15	74.12	23.31	35.36	48.23	54.21	63.68	69.66
C3C.	9.40	75.86	18.13	29.91	42.80	48.86	58.18	63.80
C3C	-32.50	70.43	23.25	35.62	48.49	54.40	63.91	69.60
O	59.55	38.47	5.23	5.08	5.01	5.01	4.98	4.98
O2	0.0	49.01	7.02	7.44	8.04	8.35	8.73	9.04
OH	9.49	43.88	7.16	7.05	7.15	7.33	7.87	8.27
H2O	-57.80	45.10	8.02	8.41	9.24	9.85	11.23	12.20
HO2	3.50	54.73	8.37	9.48	10.78	11.43	12.47	13.23
H2O2	-32.53	55.66	10.42	12.35	14.30	15.21	16.85	17.88
CO	-26.42	47.21	6.96	7.13	7.61	7.94	8.41	8.67
C.HO	10.40	53.66	8.27	9.27	10.73	11.51	12.55	13.15
HCO	10.40	53.66	8.27	9.27	10.73	11.51	12.55	13.15
CO2	-94.05	51.07	8.90	10.65	12.30	12.97	13.93	14.45
CH2O	-27.70	52.26	8.45	10.49	13.34	14.86	16.95	18.14
CH3O.	3.96	54.70	9.01	12.22	16.28	18.38	21.56	23.13
C.H2OH	-3.50	56.28	10.80	13.50	16.64	18.19	20.70	22.36
CH3OO.	3.50	64.23	13.07	17.83	22.49	24.48	27.48	29.25
C.H2OOH	11.90	65.84	13.08	17.80	22.50	24.55	27.50	28.36
CH3OOO.	7.81	73.70	17.40	22.48	27.34	29.41	32.70	34.75
CH3OH	-48.00	57.30	10.48	14.34	19.00	21.35	24.96	27.25
CH3OOH	-32.60	66.85	15.06	19.49	24.28	26.58	30.56	33.40
CH3OOOH	-29.22	76.60	19.57	24.69	29.54	31.73	36.12	39.56
CH2CO	-14.60	57.79	12.98	16.92	20.31	21.61	23.80	25.55
C*C*O	-14.60	57.79	12.98	16.92	20.31	21.61	23.80	25.55
C2H5O.	-4.10	64.63	14.09	20.20	28.02	31.17	37.06	39.72
CCO.	-4.10	64.63	14.09	20.20	28.02	31.17	37.06	39.72
C2H5OO.	-5.70	74.03	18.28	25.50	32.89	36.80	40.37	45.03
CCOO.	-5.70	74.03	18.28	25.50	32.89	36.80	40.37	45.03

CH2CH2OH	-6.90	69.95	14.71	21.16	27.38	30.05	35.90	39.00
C.CO <sub>2</sub> H	-6.90	69.95	14.71	21.16	27.38	30.05	35.90	39.00
CH2CH2OOH	8.50	78.13	19.51	27.24	33.88	36.74	40.36	45.03
C.CO <sub>2</sub> OH	8.50	78.13	19.51	27.24	33.88	36.74	40.36	45.03
CH3CHO	-39.69	63.20	13.22	18.16	24.17	27.00	30.60	34.20
CC*O	-39.69	63.20	13.22	18.16	24.17	27.00	30.60	34.20
CCOH	-56.12	67.54	15.71	22.78	30.32	33.84	39.58	43.62
CCOOH	-39.10	76.63	20.06	27.76	35.43	38.87	44.81	49.25
C2C*O	-51.56	71.46	17.96	25.92	34.87	39.19	45.97	49.84
C2*CO <sub>2</sub>	-37.40	81.44	24.98	35.95	47.28	52.68	60.13	66.44
C3CO.	-21.50	75.59	25.74	38.09	50.98	56.74	65.22	71.00
C3COO.	-21.60	82.84	31.60	44.35	56.06	60.97	69.58	75.93
C3.CO <sub>2</sub> OH	-12.20	88.66	31.60	44.35	56.06	60.97	69.58	75.93
C2.CO <sub>2</sub>	-12.36	83.40	25.99	38.29	50.18	55.55	63.73	67.79
C2C.CO <sub>2</sub>	-22.00	81.21	25.99	38.29	50.18	55.55	63.73	67.79
C2CO <sub>2</sub> .	-16.40	79.86	27.86	39.98	51.50	56.76	64.83	68.85
C2CO <sub>2</sub>	-60.90	80.86	26.77	40.00	53.28	59.31	67.85	72.23
C3COH	-77.91	78.15	27.22	40.30	53.27	59.20	69.77	76.04
C3COOH	-58.00	86.84	31.80	45.44	58.68	64.44	74.02	80.95
C3.CO <sub>2</sub>	-21.96	91.94	31.72	46.89	61.65	68.17	78.10	83.24
C3CO <sub>2</sub> .	-28.60	89.76	33.58	48.55	62.95	69.34	79.01	83.92
C3CO <sub>2</sub>	-70.00	85.84	32.49	48.51	64.66	71.96	83.06	88.68

## Appendix B

# DISSOC Input Data and Results

## B.1 $C_3COC$



k	A	Ea	source
1	7.94 E+13	59.0	a
2	4.49 E+17	79.0	b
3	2.38 E+16	81.0	c
4	3.18 E+17	82.0	d
5	3.16 E+16	98.6	e
6	8.81 E+14	92.0	f
$\nu = 1122.5 / \text{cm}$			g
LJ parameters :			h
$\sigma = 5.81 \text{ \AA}$		$e/k = 424.3 \text{ cal}$	

a. K. Y. Choo, D. M. Golden, and S. W. Benson<sup>25</sup>.

b. From  $A_{-1} = 7.94 \times 10^{12}$ , which was taken as recombination of  $CC \cdot + C_3C \cdot$  (Allara

& Shaw<sup><23></sup>) and microscopic reversibility.

$$Ea_1 = \Delta H - 2 \text{ kcal/mole.}$$

- c. From  $A_{-2} = 2.00 \times 10^{13}$ , which was taken as the average of recombinations of  $CH_3+$  primary radicals of hydrocarbons (Allara & Shaw<sup><23></sup>) and microscopic reversibility.

$$Ea_2 = \Delta H - RT \text{ kcal/mole.}$$

- d. From  $A_{-3} = 1.58 \times 10^{13}$ , which was taken as the average of recombinations of  $CH_3+$  secondary radicals of hydrocarbons (Allara & Shaw<sup><23></sup>) and microscopic reversibility.

$$Ea_3 = \Delta H - RT \text{ kcal/mole.}$$

- e. From  $A_{-4} = 1.00 \times 10^{14}$ , which was taken as the average of recombinations of  $H+$  primary radicals of hydrocarbons (Allara & Shaw<sup><23></sup>) and microscopic reversibility.

$$Ea_4 = \Delta H - RT \text{ kcal/mole.}$$

- f. From  $A_{-5} = 1.00 \times 10^{14}$ , which was taken as the average of recombinations of  $H+$  primary radicals of hydrocarbons (Allara & Shaw<sup><23></sup>) and microscopic reversibility.

$$Ea_5 = \Delta H - RT \text{ kcal/mole.}$$

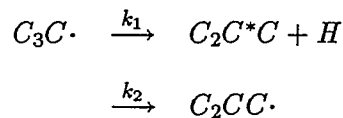
- g. From the calculation of CPFIT computer code<sup><29></sup>.

- h. Activated complex L-J parameters are estimated using critical property data tabulated in Reid, Prausnitz and Sherwood (*The Properties and Gases and Liquids*,

3rd ed.)

## Unimolecular QRRK (DISSOC) Output (800 – 1200 K)

torr	Reaction ( $N_2$ Bath)	A	$E_a$
7.6	$C_3COC \rightarrow C_2C * C + CH_3OH$	4.72E+13	58.1
76.0		6.87E+13	58.8
760.0		7.72E+13	59.0
7.6	$C_3COC \rightarrow C_3C \cdot + CH_3O \cdot$	5.07E+16	75.5
76.0		2.02E+17	77.7
760.0		3.66E+17	78.7
7.6	$C_3COC \rightarrow C_3CO \cdot + CH_3$	2.05E+15	77.0
76.0		9.48E+15	79.5
760.0		1.87E+16	80.6
7.6	$C_3COC \rightarrow C_2C \cdot OC + CH_3$	2.65E+16	78.0
76.0		1.17E+17	80.4
760.0		2.39E+17	81.5
7.6	$C_3COC \rightarrow C_3 \cdot COC + H$	4.03E+14	93.7
76.0		4.57E+15	97.5
760.0		1.72E+16	99.7
7.6	$C_3COC \rightarrow C_3COC \cdot + H$	3.99E+13	89.0
76.0		2.48E+14	91.9
760.0		6.13E+14	93.4

B.2  $C_3C\cdot$ 

k	A	Ea	source
1	5.40 E+13	38.3	a
2	4.31 E+13	42.5	b
$\nu = 1377.8$ /cm			c
LJ parameters :			d
$\sigma = 5.19\text{\AA}$		$\epsilon/k = 339.7$ cal	

a. From Dean's estimation<sup><21></sup> of  $A_i/\#H = 6 \times 10^{12} s^{-1}$  and  $E_i = \Delta H + 2.5$  kcal/mole for C-H rupture in primary hydrocarbon radicals.

b. From Transition State Theory for loss of one rotor, symmetry

$$A_2 = 10^{13.56} \times 10^{\Delta S/4.6} \times \text{degeneracy}$$

$$\Delta S = -4.0, \text{ degeneracy} = 9.$$

$$Ea_2 = 27.6 + 4.49 + 10.4 (\text{Ring strain} + \Delta H_{rxn} + Ea_{abstraction}).$$

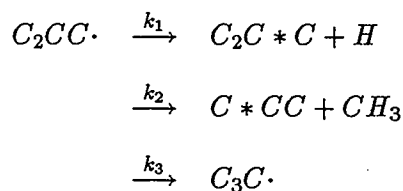
c. From the calculation of CPFIT computer code<sup><29></sup>.

d. Activated complex L-J parameters are estimated using critical property data tabulated in Reid, Prausnitz and Sherwood (*The Properties and Gases and Liquids, 3rd ed.*)

Apparent Reaction Rate Constants Predicted by  
Unimolecular QRRK (DISSOC) Analysis (800 – 1200 K)

P	Reaction	A	Ea
(torr)		(s <sup>-1</sup> )	(Kcal/mol)
7.6	$C_3C\cdot \rightarrow C_2C^*C + H$	2.49E+11	30.2
76.0		4.01E+12	34.2
760.0		2.35E+13	37.0
7.6	$C_3C\cdot \rightarrow C_2CC\cdot$	6.38E+10	33.1
76.0		1.53E+12	37.4
760.0		1.37E+13	40.7

### B.3 $C_2CC\cdot$



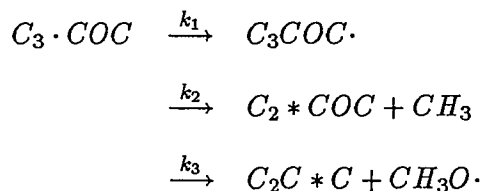
k	A	Ea	source
1	6.00 E+12	31.8	a
2	4.00 E+13	31.9	b
3	9.31 E+13	38.0	c
$\nu = 1229.5 / \text{cm}^{-1}$			d
LJ parameters :			e
$\sigma = 5.19 \text{ \AA}$	$e/k = 339.7 \text{ cal}$		

- a. Based upon Dean's estimation<sup><21></sup> of  $A_i/\#H = 6 \times 10^{12} \text{ s}^{-1}$  and  $E_i = \Delta H + 2.5$  kcal/mole and 1.0 kcal for C-H rupture in primary and secondary hydrocarbon radicals respectively.
- $A_1 = 6 \times 10^{12} \text{ s}^{-1}$  and  $E_{a_1} = \Delta H + 0.5$  kcal/mole.
- b. From Dean's estimation<sup><21></sup> of  $A_i = 2 \times 10^{13} \text{ s}^{-1}$  for C-C rupture in hydrocarbon radicals and  $E_{a_2} = \Delta H + 9.0$  kcal/mole from Allara & Show<sup><23></sup>.
- c. Microscopic reversibility from reaction described in B.2-b.
- d. From the calculation of CPFIT computer code<sup><29></sup>.

- e. Activated complex L-J parameters are estimated using critical property data tabulated in Reid, Prausnitz and Sherwood (*The Properties and Gases and Liquids*, 3rd ed.)

Apparent Reaction Rate Constants Predicted by  
Unimolecular QRRK (DISSOC) Analysis (800 – 1200 K)

P (torr)	Reaction	A (s <sup>-1</sup> )	Ea (Kcal/mol)
7.6	$C_2CC\cdot \rightarrow C_2C^*C + H$	2.64E+09	20.7
76.0		7.31E+10	25.1
760.0		9.97E+11	29.0
7.6	$C_2CC\cdot \rightarrow C^*CC + CH_3$	1.67E+10	20.8
76.0		4.70E+11	25.2
760.0		6.51E+12	29.1
7.6	$C_2CC\cdot \rightarrow C_3C\cdot$	7.25E+09	25.3
76.0		2.68E+11	29.4
760.0		6.62E+12	33.9

B.4  $C_3 \cdot COC$ 

k	A	Ea	source
1	7.13 E+11	18.6	a
2	1.44 E+14	30.1	b
3	1.29 E+15	28.5	c
$\nu = 1103.7 / \text{cm}$	*		d
LJ parameters :			e
$\sigma = 5.81 \text{ \AA}$	$e/k = 424.3 \text{ cal}$		

a. From Transition State Theory for loss of 3 rotors.

$$A_1 = 10^{13.56} \times 10^{\Delta S/4.6} \times \text{degeneracy}$$

$$\Delta S = -10.0, \text{ degeneracy} = 3.$$

$$Ea_1 = 6.3 + 12.3 (\text{Ring strain} + Ea_{\text{abstraction}}).$$

b. From  $A_{-2} = 2.51 \times 10^{11}$ , which was taken as addition of  $CH_3+$  olefin (Allara & Shaw<sup><23></sup>) and microscopic reversibility.

$$Ea_2 = \Delta H + 10.7 \text{ kcal/mole.}$$

c. From  $A_{-3} = 3.98 \times 10^{10}$ , which was taken as addition of  $CC \cdot$  + olefin (Allara &

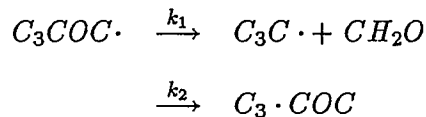
Shaw<sup><23></sup>) and microscopic reversibility.

$$Ea_2 = \Delta H + 9.2 \text{ kcal/mole.}$$

- d. From the calculation of CPFIT computer code<sup><29></sup>.
- e. Activated complex L-J parameters are estimated using critical property data tabulated in Reid, Prausnitz and Sherwood (*The Properties and Gases and Liquids*, 3rd ed.)

Apparent Reaction Rate Constants Predicted by  
Unimolecular QRRK (DISSOC) Analysis (800 - 1200 K)

P (torr)	Reaction	A (s <sup>-1</sup> )	Ea (Kcal/mol)
7.6	$C_3 \cdot COC \rightarrow C_3COC \cdot$	3.31E+06	0.90
76.0		1.48E+08	5.78
760.0		5.29E+09	10.9
7.6	$C_3 \cdot COC \rightarrow C_2^*COC + CH_3$	4.36E+07	10.9
76.0		1.52E+09	14.1
760.0		8.66E+10	17.9
7.6	$C_3 \cdot COC \rightarrow C_2C^*C + CH_3O \cdot$	4.88E+08	9.25
76.0		1.90E+10	12.8
760.0		1.09E+12	17.9

B.5  $C_3COC\cdot$ 

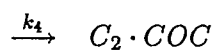
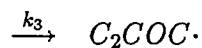
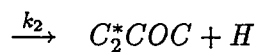
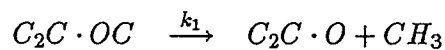
k	A	Ea	source
1	1.46 E+14	20.1	a
2	2.14 E+12	23.3	b
$\nu = 1048.1 / \text{cm}$			c
LJ parameters :			d
$\sigma = 5.81 \text{ \AA}$		$\epsilon/k = 424.3 \text{ cal}$	

- a. From  $A_{-1} = 3.98 \times 10^{10}$ , which was taken as addition of  $CC\cdot CC + C^*C$  (Allara & Shaw<sup><23></sup>) and microscopic reversibility.
- $Ea_1 = \Delta H + 6.9 \text{ kcal/mole.}$
- b. Microscopic reversibility from reaction described in B.4-a.
- c. From the calculation of CPFIT computer code<sup><29></sup>.
- d. Activated complex L-J parameters are estimated using critical property data tabulated in Reid, Prausnitz and Sherwood (*The Properties and Gases and Liquids, 3rd ed.*)

Apparent Reaction Rate Constants Predicted by  
Unimolecular QRRK (DISSOC) Analysis (800 – 1200 K)

P (torr)	Reaction	A (s <sup>-1</sup> )	Ea (Kcal/mol)
7.6	$C_3COC \cdot \longrightarrow C_3C \cdot + CH_2O$	1.85E+07	0.82
76.0		5.59E+08	3.48
760.0		3.02E+10	7.83
7.6	$C_3COC \cdot \longrightarrow C_3 \cdot + COC$	3.56E+05	5.70
76.0		6.95E+06	7.29
760.0		2.84E+08	10.8

## B.6 $C_2C \cdot OC$



k	A	Ea	source
1	5.89 E+13	12.1	a
2	3.60 E+13	39.2	b
3	2.49 E+12	42.2	c
4	2.87 E+13	47.6	d
$\nu = 1083.6 / \text{cm}$			e
LJ parameters :			f
$\sigma = 5.39 \text{ \AA}$		$e/k = 395.1 \text{ cal}$	

a. From  $A_{-1} = 2.51 \times 10^{11}$  and  $Ea_{-1} = 7.3 \text{ kcal/mole}$ , which were taken as the average of additions of  $CH_3 + C_3H_6$  and  $CH_3 + 1 - C_4H_8$  (Allara & Shaw<sup><23></sup>) and microscopic reversibility.

b. From Dean's estimation<sup><21></sup> of  $A_i/\#H = 6 \times 10^{12} \text{ s}^{-1}$  and  $E_i = \Delta H + 2.5 \text{ kcal/mole}$  for C-H rupture in primary hydrocarbon radicals.

c. From Transition State Theory for loss of 2 rotors, symmetry.

$$A_3 = 10^{13.56} \times 10^{\Delta S/4.6} \times \text{degeneracy}$$

$$\Delta S = -7.5, \text{ degeneracy} = 3.$$

$$Ea_1 = 26.2 + 5.6 + 10.4 \text{ (Ring strain} + \Delta H_{rxn} + Ea_{abstraction}).$$

- d. From Transition State Theory for loss of one rotor, symmetry

$$A_3 = 10^{13.56} \times 10^{\Delta S/4.6} \times \text{degeneracy}$$

$$\Delta S = -4.0, \text{ degeneracy} = 6.$$

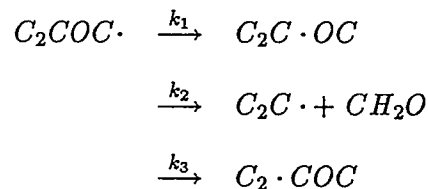
$$Ea_1 = 27.6 + 9.6 + 10.4 \text{ (Ring strain} + \Delta H_{rxn} + Ea_{abstraction}).$$

- e. From the calculation of CPFIT computer code<sup><29></sup>.

- f. Activated complex L-J parameters are estimated using critical property data tabulated in Reid, Prausnitz and Sherwood (*The Properties and Gases and Liquids*, 3rd ed.)

Apparent Reaction Rate Constants Predicted by  
Unimolecular QRRK (DISSOC) Analysis (800 – 1200 K)

P (torr)	Reaction	A ( $s^{-1}$ )	Ea (Kcal/mol)
7.6	$C_2C\cdot \rightarrow C_2C^*O + CH_3$	5.12E+06	-1.98
76.0		5.51E+07	-1.81
760.0		8.18E+08	-0.87
7.6	$C_2C\cdot \rightarrow C_2^*COC + H$	1.31E+07	32.1
76.0		1.31E+08	32.1
760.0		1.31E+09	32.1
7.6	$C_2C\cdot \rightarrow C_2COC\cdot$	9.16E+05	35.4
76.0		9.16E+06	35.4
760.0		9.20E+07	35.4
7.6	$C_2C\cdot \rightarrow C_2\cdot COC$	1.07E+07	41.3
76.0		1.07E+08	41.3
760.0		1.07E+09	41.3

B.7  $C_2COC$ .

k	A	Ea	source
1	4.91 E+12	16.7	a
2	3.39 E+14	17.9	b
3	1.43 E+12	20.7	c
$\nu = 1017.4 / \text{cm}$			d
LJ parameters :			e
$\sigma = 5.39 \text{ \AA}$		$e/k = 395.1 \text{ cal}$	

- a. Microscopic reversibility from reaction described in B.6-c.
- b. From  $A_{-2} = 3.98 \times 10^{10}$ , which was taken as addition of  $CC \cdot C + C^*C$  (Allara & Shaw<sup><23></sup>) and microscopic reversibility.
- $$Ea_2 = \Delta H + 6.9 \text{ kcal/mole.}$$

- c. From Transition State Theory for loss of 3 rotors, symmetry

$$A_3 = 10^{13.56} \times 10^{\Delta S/4.6} \times \text{degeneracy}$$

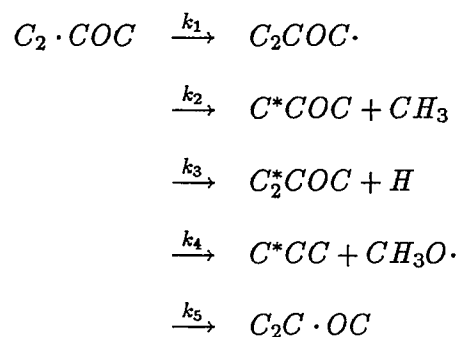
$$\Delta S = -10.0, \text{ degeneracy} = 6.$$

$$Ea_1 = 6.3 + 4.0 + 10.4 \text{ (Ring strain} + \Delta H_{rxn} + Ea_{abstraction}).$$

- d. From the calculation of CPFIT computer code<sup><29></sup>.
- e. Activated complex L-J parameters are estimated using critical property data tabulated in Reid, Prausnitz and Sherwood (*The Properties and Gases and Liquids, 3rd ed.*)

Apparent Reaction Rate Constants Predicted by  
Unimolecular QRRK (DISSOC) Analysis (800 – 1200 K)

P (torr)	Reaction	A (s <sup>-1</sup> )	Ea (Kcal/mol)
7.6	$C_2COC \cdot \longrightarrow C_2C \cdot OC$	6.60E+04	-4.00
76.0		2.22E+06	-0.96
760.0		7.17E+07	1.99
7.6	$C_2COC \cdot \longrightarrow C_2C \cdot + CH_2O$	1.36E+07	0.37
76.0		1.82E+08	1.06
760.0		4.49E+09	3.30
7.6	$C_2COC \cdot \longrightarrow C_2 \cdot COC$	9.11E+04	5.30
76.0		9.96E+05	5.51
760.0		1.64E+07	6.72

B.8  $C_2 \cdot COC$ 

k	A	Ea	source
1	2.41 E+11	16.7	a
2	1.71 E+14	30.4	b
3	6.00 E+12	27.6	c
4	6.40 E+12	30.3	d
5	9.52 E+12	38.0	e
$\nu = 1114.4 / \text{cm}$			f
LJ parameters :			g
$\sigma = 5.39 \text{ \AA}$	$e/k = 395.1 \text{ cal}$		

a. Microscopic reversibility from reaction described in B.6-d.

b. From  $A_{-2} = 2.51 \times 10^{11}$  and  $Ea_{-2} = 9.0 \text{ kcal/mole}$ , which were taken as the average of additions of  $CH_3 + C_3H_6$  and  $CH_3 + 1 - C_4H_8$  (Allara & Shaw<sup><23></sup>) and microscopic reversibility.

c. Taken as  $C_2 \cdot CCC \rightarrow C_2^*CCC + H$  from Dean<sup><23></sup>.

$$Ea_3 = \Delta H + 0.5 \text{ kcal/mole.}$$

d. From  $A_{-4} = 3.98 \times 10^{10}$  and  $Ea_{-4} = 9.2 \text{ kcal/mole}$ , which were taken as the average of additions of  $CC \cdot + C_3H_6$  and  $CC \cdot + 1 - C_4H_8$  (Allara & Show<sup><23></sup>) and microscopic reversibility.

e. Microscopic reversibility from reaction described in B.7.

f. From the calculation of CPFIT computer code<sup><29></sup>.

g. Activated complex L-J parameters are estimated using critical property data tabulated in Reid, Prausnitz and Sherwood (*The Properties and Gases and Liquids*, 3rd ed.)

Apparent Reaction Rate Constants Predicted by  
Unimolecular QRRK (DISSOC) Analysis (800 – 1200 K)

P (torr)	Reaction	A ( $s^{-1}$ )	Ea (Kcal/mol)
7.6	$C_2 \cdot COC \longrightarrow C_2COC \cdot$	5.64E+07	4.86
76.0		2.17E+09	9.54
760.0		3.47E+10	13.6
7.6	$C_2 \cdot COC \longrightarrow C^*COC + CH_3$	3.36E+09	17.1
76.0		9.19E+10	19.9
760.0		3.47E+12	24.5
7.6	$C_2 \cdot COC \longrightarrow C_2^*COC + H$	1.75E+08	14.3
76.0		5.60E+09	17.6
760.0		1.91E+11	22.3
7.6	$C_2 \cdot COC \longrightarrow C^*CC + CH_3O \cdot$	1.39E+08	17.1
76.0		3.84E+09	19.9
760.0		1.42E+11	24.5
7.6	$C_2 \cdot COC \longrightarrow C_2C \cdot OC + CH_3O$	9.26E+07	25.1
76.0		1.68E+09	26.6
760.0		6.44E+10	30.7